Ultrafast glutamate sensors resolve high-frequency release at Schaffer collateral synapses

Nordine Helassa[1], Celine Durst[2], Catherine Coates[1], Silke Kerruth[1], Urwa Arif[1], Christian Schulze[2], J. Simon Wiegert[2], Michael Geeves[3], Thomas Oertner[2], Katalin Torok[1]

[1]St George's, University of London, [2]Center for Molecular Neurobiology Hamburg, [3]University of Kent

Submitted to Proceedings of the National Academy of Sciences of the United States of America

Glutamatergic synapses display a rich repertoire of plasticity mechanisms on many different time scales, involving dynamic changes in the efficacy of transmitter release as well as changes in the number and function of postsynaptic glutamate receptors. The genetically encoded glutamate sensor iGluSnFR enables visualization of glutamate release from presynaptic terminals at frequencies up to ~10 Hz. However, to resolve glutamate dynamics during high frequency bursts, faster indicators are required. Here we report the development of fast (iGlu$_f$) and ultrafast (iGlu$_u$) variants with comparable brightness, but increased K_d for glutamate (137 μM and 600 μM, respectively). Compared to iGluSnFR, iGlu$_u$ has a 6-fold faster dissociation rate *in vitro* and 5-fold faster kinetics in synapses. Fitting a three-state model to kinetic data, we identify the large conformational change after glutamate binding as the rate-limiting step. In rat hippocampal slice culture stimulated at 100 Hz, we find that iGlu$_u$ is sufficiently fast to resolve individual glutamate release events, revealing that glutamate is rapidly cleared from the synaptic cleft. Depression of iGlu$_u$ responses during 100 Hz trains correlates with depression of postsynaptic EPSPs, indicating that depression during high frequency stimulation is purely presynaptic in origin. At individual boutons, the recovery from depression could be predicted from the amount of glutamate released on the second pulse (paired pulse facilitation/depression), demonstrating differential frequency-dependent filtering of spike trains at Schaffer collateral boutons.

glutamate | synaptic transmission | post-tetanic potentiation | hippocampus | two-photon imaging

Introduction

The efficacy of synaptic transmission is not constant, but changes dynamically during high-frequency activity. In terms of information processing, different forms of short-term plasticity act as specific frequency filters: facilitating synapses are most effective during high frequency bursts, while depressing synapses preferentially transmit isolated spikes preceded by silent periods (1). Mechanistically, a number of pre- and postsynaptic parameters change dynamically during high frequency activity, e.g. the number of readily releasable vesicles, presynaptic Ca^{2+} dynamics, and the properties of postsynaptic receptors, which may be altered by Ca^{2+}-activated enzymes (2, 3).

Electrophysiological analysis of short-term plasticity, by monitoring postsynaptic responses, is complicated by the fact that neurons are often connected by more than one synapse. In addition, it is not straightforward to distinguish between pre- and postsynaptic plasticity mechanisms. Directly measuring glutamate concentrations inside the synaptic cleft during high-frequency activity would allow isolating the dynamics of the vesicle release machinery from potential changes in glutamate receptor properties (e.g. desensitization, phosphorylation or lateral diffusion). Early fluorescent glutamate sensors, constructed by chemical labelling of the fused glutamate binding lobes of ionotropic glutamate receptor GluA2 (termed S1S2) (4-6) and later of the bacterial periplasmic glutamate/aspartate binding protein (GluBP) (7, 8), were not suitable for quantitative single-synapse experiments due to their low dynamic range. Genetically encoded FRET-based fluorescent glutamate sensors e.g. FLIPE, GluSnFR and Super-GluSnFR (**Fig. 1a**) have relatively low FRET efficiency, since glutamate binding causes only a small conformational change in GluBP (9-11). A breakthrough in visualizing glutamate release in intact tissue was achieved with iGluSnFR, a single-fluorophore glutamate sensor (12). Following the concept developed for the GCaMP family of genetically encoded Ca^{2+} sensors (13), iGluSnFR was constructed from circularly permuted (cp) EGFP (14) inserted into the GluBP sequence, creating a large fragment iGlu$_l$ (residues 1-253) at the N-terminus and a small fragment iGlu$_s$ (residues 254-279) at the C-terminus (**Fig. 1a**). Upon glutamate binding GluBP is reconstituted from its two fragments, pulling the cpEGFP β-barrel together, resulting in a ~5-fold fluorescence increase. iGluSnFR is targeted for extracellular expression, like previous genetically encoded glutamate sensors, by fusion with a PDGFR peptide segment (10, 12).

iGluSnFR has high glutamate affinity and a large dynamic range, but reacts relatively slowly to synaptic glutamate release with a reported decay half-time ($t_{1/2}$) of 92 ms (12). Imaging iGluSnFR in cultured hippocampal neurons during 10 Hz stimulation shows summation, which, without deconvolution, might indicate that glutamate accumulates during stimulation (15). Deconvolution of the data suggests that glutamate is cleared between release events (15). Here we introduce two fast iGluSnFR variants, iGlu$_f$ (for 'fast') and iGlu$_u$ (for 'ultrafast') for accurate tracking of synaptic glutamate dynamics during high frequency transmission and identify the rate-limiting step leading to bright fluorescence upon glutamate binding. In organotypic

Significance

Excitatory synapses convert presynaptic action potentials into chemical signals that are sensed by postsynaptic glutamate receptors. To eavesdrop on synaptic transmission, genetically encoded fluorescent sensors for glutamate have been developed. However, even the best available sensors lag behind the very fast glutamate dynamics in the synaptic cleft. Here we report the development of an ultrafast genetically encoded glutamate sensor, iGlu$_u$, which allowed us to image glutamate clearance and synaptic depression during 100 Hz spike trains. We found that only boutons showing paired-pulse facilitation were able to rapidly recover from depression. Thus, presynaptic boutons act as frequency-specific filters to transmit select features of the spike train to specific postsynaptic cells.

Reserved for Publication Footnotes

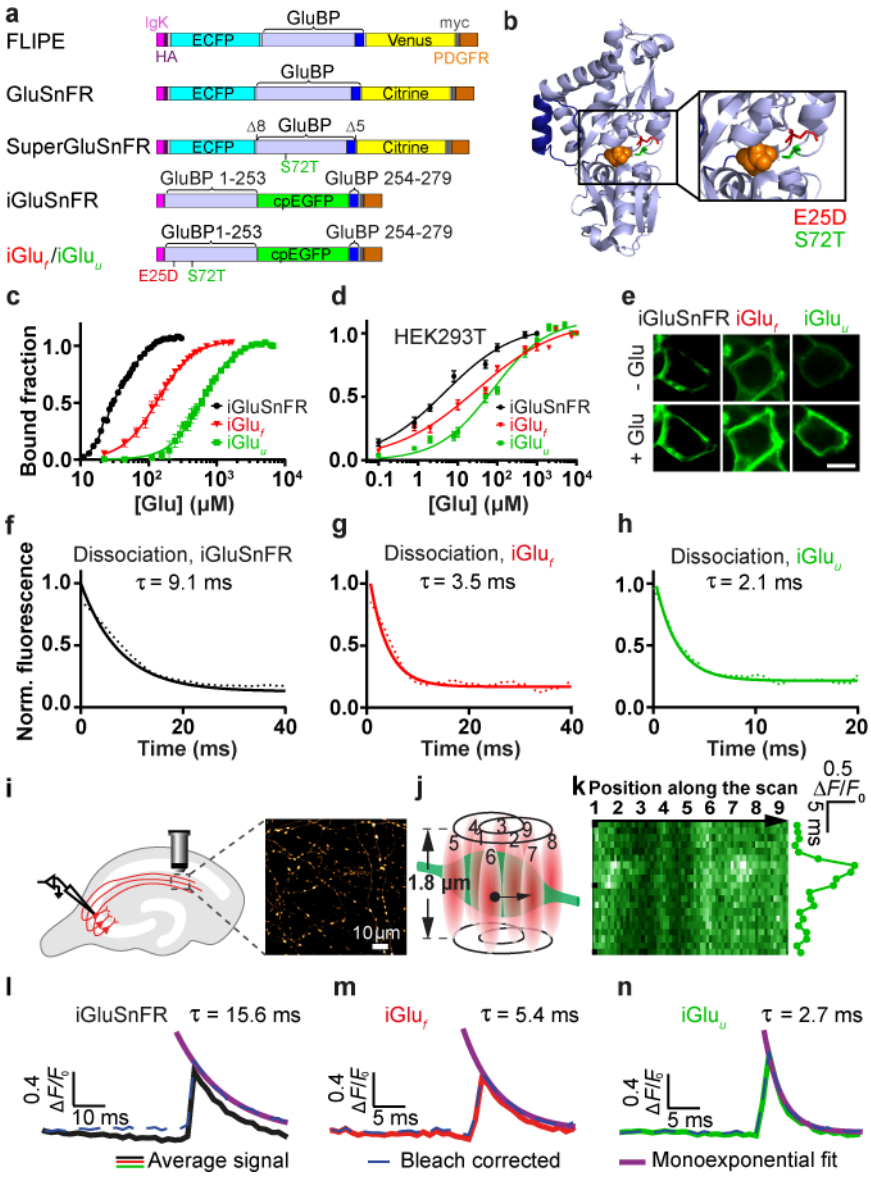

Fig. 1. Genetically encoded glutamate indicators (GEGI). (**a**) Domain structure and design of FRET- and single fluorophore-based GEGI; key: (GluBP) (blue), cpEGFP (green), IgG kappa secretion tag (pink), hemagglutinin (HA) tag (purple), myc tag (grey) and a PDGFR transmembrane domain (brown); GluBP 1-253 and 254-279 fragments are in light and dark blue, respectively; ▵8 aa and ▵5 aa specify deletions at the N- and C-terminus of GluBP introduced in GluSnFR. (**b**) Design of selected iGluSnFR variants. Crystal structure of GluBP (PDB 2VHA, adapted from (8). Selected mutated residues around the glutamate site are shown as red and green backbone. Bound glutamate is represented in orange space filling display. (**c**) Equilibrium glutamate binding titrations at 20 °C for iGluSnFR (●), iGluSnFR E25D (iGlu$_f$) (▾) and iGluSnFR S72T (iGlu$_u$) (■) *in vitro*; (**d**) Glutamate titrations *in situ* at 37 °C. iGluSnFR, iGlu$_f$ and iGlu$_u$ were expressed in HEK293T cells and titrated with glutamate. Data derived from iGluSnFR (n = 19), iGlu$_f$ (n = 41) and iGlu$_u$ (n = 33). (**e**) Representative images of HEK293T cells prior to glutamate addition and at saturating (1, 3 and 10 mM, respectively) glutamate. The scale bar represents 10 μm. Glutamate dissociation kinetics of (**f**) iGluSnFR, (**g**) iGlu$_f$and (**h**) iGlu$_u$ determined by stopped-flow fluorimetry. Experimental data (dotted lines) are overlaid by curves fitted to single exponentials (solid lines). Fluorescence changes are normalised to F_{max} of 1. Imaging glutamate release from single presynaptic terminals. (**i**) Schematic representation of hippocampal slice with transfected and patch-clamped CA3 pyramidal cell. (**j**) Spiral scan intersecting site of vesicular fusion. (**k**) Zoomed-in image of single trial iGlu$_u$ response. Decay time (τ_{off}) measurements with bleach correction (solid lines) for individual experiments by single exponential fit for (**l**) iGluSnFR (n = 13 boutons, 500 Hz sampling rate) and variants (**m**) iGlu$_f$ (n = 7 boutons, 1 kHz sampling rate) and (**n**) iGlu$_u$ (n = 7 boutons, 1 kHz sampling rate).

slice cultures of rat hippocampus, iGlu$_u$ directly reports discrete synaptic glutamate release events at 100 Hz. Combining high-speed two-photon imaging and electrophysiology, we show that short-term depression of Schaffer collateral AMPA responses is fully accounted for by the depression of glutamate release. Furthermore, we show a tight correlation between paired-pulse facilitation and rapid recovery from post-tetanic depression at individual boutons, suggesting that differential use of presynaptic resources (readily releasable vesicles) determines the filtering properties of CA3 pyramidal cell boutons.

Results

Affinity variants of iGluSnFR by binding site mutations. We generated six iGluSnFR variants by mutating residues coordinating glutamate or in the vicinity of the binding site (9). Two of the mutations lowered, and four increased, the K_d for glutamate. Variants in order of increasing K_d were E25A<E25R<iGluSnFR<E25D<S72T<R24K<T92A (from 19 μM to 12 mM) with Hill coefficients of 1.3 to 2.6 (**SI Appendix Fig. S1a** and **Table S1**).

We selected the two variants with the fastest response kinetics, iGluSnFR E25D (termed iGlu$_f$) and iGluSnFR S72T (termed iGlu$_u$) (**Fig. 1a,b**) for detailed biophysical characterization as isolated proteins and as membrane-bound glutamate sensors on HEK293T cells and pyramidal neurons. Selectivity for glutamate was determined against aspartate, glutamine, D-serine, GABA and glycine. iGlu$_f$ and iGlu$_u$ affinities for aspartate were similar to that for glutamate, as previously reported for iGluSnFR (12), but with 2 to 3-fold lower fluorescence enhancement. The affinity for glutamine was in the mM range for all three probes (**SI Appendix Fig. S1b, Table S3**). D-serine, GABA and glycine evoked no detectable response. pK_a for the glutamate-bound form was ~ 6.5 for iGluSnFR iGlu$_f$ and iGlu$_u$, whereas the apo-form showed little pH dependence indicating a well-shielded chromophore (**SI Appendix Fig. S1c-e**). Brightness values for iGlu$_f$ and iGlu$_u$ were similar to that for iGluSnFR (**SI Appendix Table S2**). *In vitro* measurements gave a dissociation constant (K_d) for glutamate of 33 μM for iGluSnFR, similar to that previously reported (12), while iGlu$_f$ and iGlu$_u$ had increased K_d values of 137 μM and 600 μM, respectively (**Fig. 1c, SI Appendix Table S1**). When expressed on the membrane of HEK293T cells, K_d values for glutamate were reduced to 3.1 ± 0.3 μM for iGluSnFR, 26 ± 2 μM for

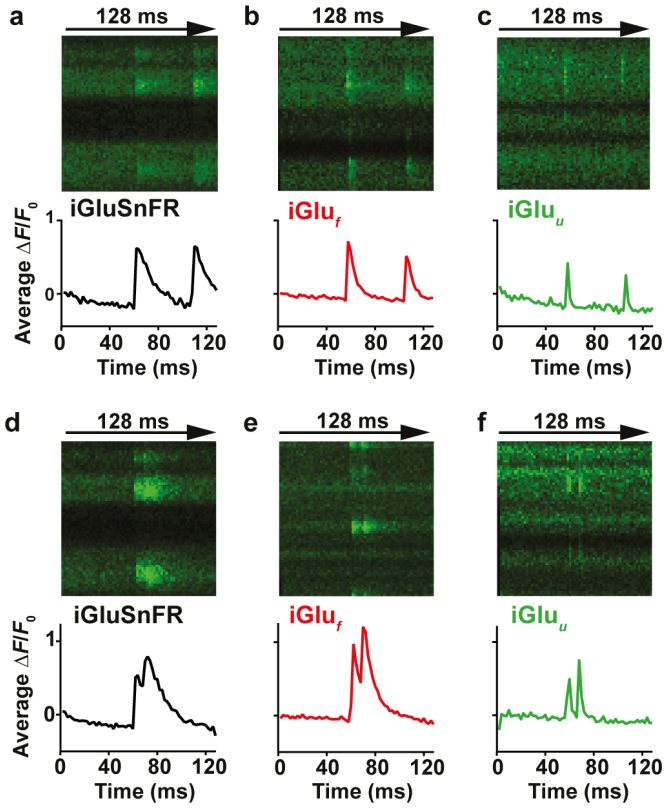

Fig. 2. Imaging glutamate release from single presynaptic terminals. Spiral line scans at 500 Hz were used to cover the entire surface of individual boutons, intersecting the release site multiple times. Averages of 3-6 responses of (**a, d**) iGluSnFR, (**b, e**) iGlu$_f$ and (**c, f**) iGlu$_u$-expressing boutons stimulated by 2 somatic APs at 48 ms (**a-c**) and 10 ms inter-stimulus intervals (**d-f**).

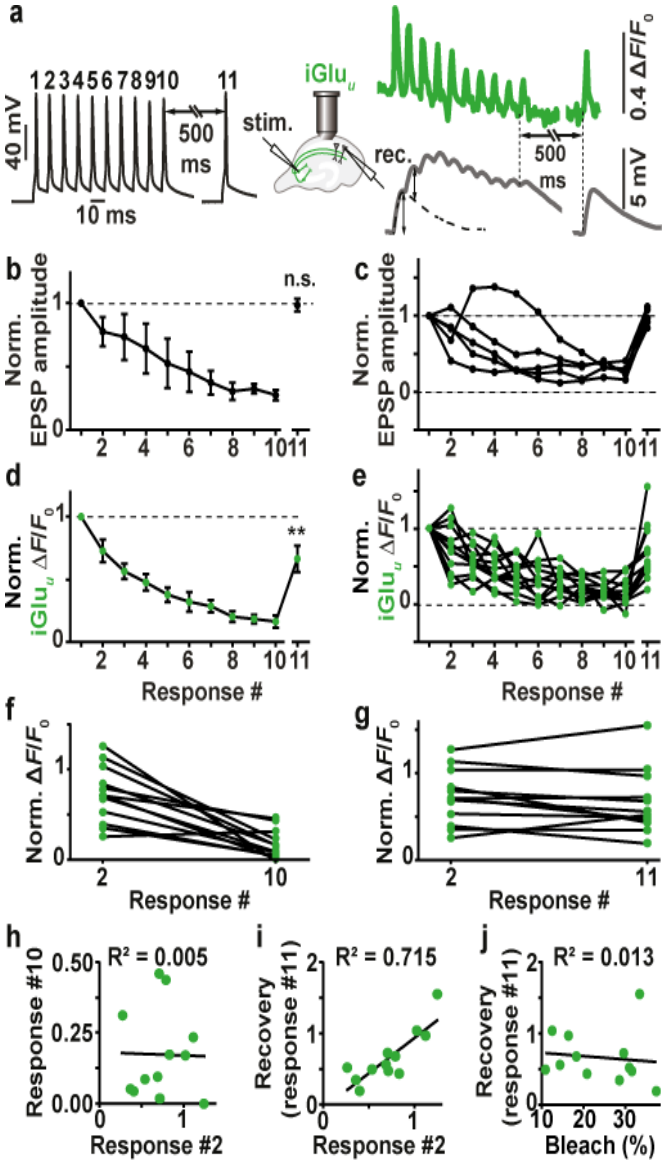

Fig. 3. Depression and recovery of synaptic transmission during 100 Hz trains. (**a**) Example of patch-clamp recording from a connected pair of CA3-CA1 pyramidal cells. Black trace: induced action potentials (APs) in CA1 pyramidal cell, 100 Hz train and single AP. Gray trace: EPSPs in CA1 pyramidal cell (average of 50 sweeps). The single AP response (right) was used to extract EPSP amplitudes from the burst response (dotted line). Green trace: average of 10 sweeps of single-bouton iGlu$_u$ responses to identical stimulation. (**b**) EPSPs (deconvoluted amplitudes) show strong depression during the 100 Hz train, followed by full recovery 500 ms later (n = 5 CA3-CA1 pairs); two-tailed student's test comparing EPSP #1 and EPSP #11. (**c**) Individual paired recordings show consistent depression (response #10) and recovery (response #11). (**d**) Glutamate release shows strong depression during the 100 Hz train and partial recovery 500 ms later (n = 12 boutons, 8 cells); two-tailed student's test comparing response #1 and response #11 (*p*-value: 0.0034). (**e**) Individual Schaffer collateral boutons show large variability in response #2 and in recovery response (#11) (**f**) responses by iGlu$_u$ to the second AP (paired-pulse facilitation/depression) were not correlated with total depression (response #10 normalized to response #1). (**g**) iGlu$_u$ responses to the second AP (response #2 normalized to response #1) were highly correlated with recovery after 500 ms (response #11 normalized to response #1). Recovery was independent of indicator bleach ($F_{0,\ \text{response \#11}}$/ $F_{0,\ \text{response \#1}}$).

iGlu$_f$ and 53 ± 4 μM for iGlu$_u$ (measured at 37 °C, **Fig. 1d,e**). A similar reduction of the K_d in the cellular environment compared to that in solution was reported for iGluSnFR (12). The *in situ* fluorescence dynamic range (F_{+Glu} - F_{-Glu})/F_{-Glu} or $^{\triangle}F/F_0$) was 1.0 ± 0.1 for both iGluSnFR and iGlu$_f$, but 1.7-fold larger for iGlu$_u$.

Kinetic measurements of iGluSnFR variants in vitro and in situ. Based on their large K_d values, we expected iGlu$_f$ and iGlu$_u$ to have faster glutamate release kinetics than iGluSnFR. Fluorescence measurements in a stopped-flow instrument indeed revealed faster *off*-rates for the new variants: using the non-fluorescent high-affinity GluBP 600n (10) in excess (0.67 mM) to trap released glutamate, k_{off} values of 110 s^{-1} (τ_{off} = 9 ms), 283 s^{-1} (τ_{off} = 4 ms) and 468 s^{-1} (τ_{off} = 2 ms) were obtained for iGluSnFR, iGlu$_f$ and iGlu$_u$, respectively, at 20 °C (**Fig. 1f-h** and **SI Appendix Table S4**). To compare *in vitro* response kinetics to physiological measurements, the temperature dependencies of the *off*-rates of iGluSnFR and the fast variants were determined. Linear Arrhenius plots were obtained between 4 °C and 34 °C (**SI Appendix Fig. S1f,g**). For the fast variants, values exceeding the temporal precision of our stopped-flow device were linearly extrapolated. At 34 °C, decay rates were 233 ± 3 s^{-1} for iGluSnFR (τ_{off} = 4.3 ms), 478 ± 5 s^{-1} for iGlu$_f$ (τ_{off} = 2.1 ms) and 1481 ± 74 s^{-1} iGlu$_u$ (τ_{off} = 0.68 ms). Thus, we were able to improve iGluSnFR kinetics by a factor of 6.3.

To image glutamate dynamics in the synaptic cleft, we expressed the newly generated iGluSnFR variants in CA3 pyramidal cells in organotypic slice culture of rat hippocampus. Fluorescence was monitored at single Shaffer collateral terminals in CA1 by spiral scanning (**Fig. 1i,j**) while APs were triggered by brief (2 ms) depolarizing current injections into the soma of the transfected CA3 neuron. A zoomed-in iGlu$_u$ example trace sampled at 1 kHz, the resolution used in all quantitative experiments with this indicator, is shown (**Fig. 1k**) along with a three-

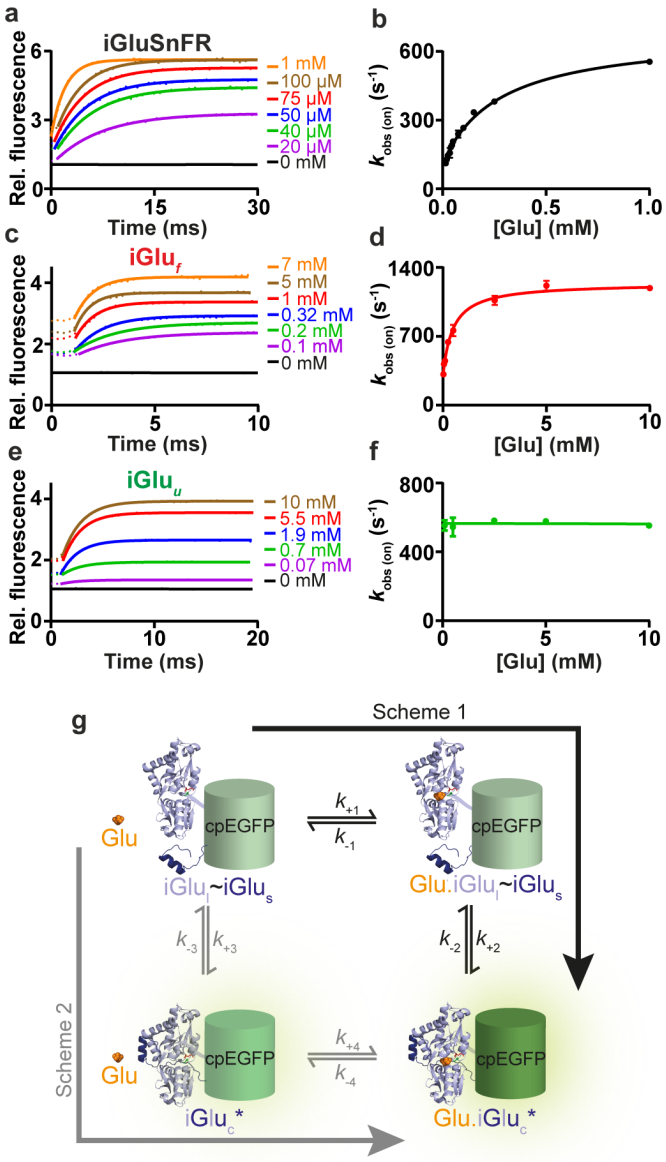

Fig. 4. Kinetics of glutamate binding by iGluSnFR variants (20 °C). (**a, c, e**) Glutamate association kinetics of iGluSnFR, $iGlu_f$and $iGlu_u$, respectively. Stopped-flow records of iGluSnFR, $iGlu_f$and $iGlu_u$ reacting with the indicated concentrations of glutamate. Experimental data (dotted lines) are overlaid with curves fitted to single exponentials (solid lines); (**b, d, f**) Plot of observed association rates, $k_{obs(on)}$ of iGluSnFR, $iGlu_f$and $iGlu_u$ as a function of glutamate concentration; (**g**) Cartoon diagram depicting the putative molecular transitions of iGluSnFR and its fast variants to the fluorescent state. Key: cpEGFP (green), GluBP 1-253 ($iGlu_l$) (light blue) and 254-279 ($iGlu_s$) (dark blue) fragments, glutamate (orange).

dimensional schematic of the scanning method. The iGluSnFR response started 4.5 ± 1.6 ms (mean ± SD) after the peak of the somatic action potential, consistent with a short propagation delay between CA3 and CA1. Consistent with the stochastic nature of glutamate release, individual boutons showed different release probabilities (median p_r = 0.56, range 0.05 – 1.0). For kinetic analysis, boutons with high release probability and good separation between release failures and successes were selected (**SI Appendix Fig. S2**). The measured fluorescence decay time constants (τ_{off}) were 13.8 ± 3.8 ms for iGluSnFR, 5.2 ± 2.0 ms for $iGlu_f$, and 2.6 ± 1.0 ms for $iGlu_u$ (**Fig. 1l-n, SI Appendix Fig. S3**). Thus, compared to iGluSnFR, synaptic responses detected by $iGlu_u$ were revealed to be faster by a factor of 5.3. Interestingly, blocking glutamate uptake with TBOA (40 µM) did not slow down the decay of $iGlu_u$ fluorescence (**SI Appendix Fig. S4**), suggesting that after sparse activation of Schaffer collateral synapses, glutamate is rapidly cleared from the synaptic cleft by diffusion, not by active transport. The situation may be different in highly active neuropil (12, 16).

Synaptic glutamate dynamics during high frequency stimulation. With decay kinetics of 1-2 ms, $iGlu_f$ and $iGlu_u$ are promising tools for direct tracking of synaptic glutamate during high frequency stimulation. The response of iGluSnFR, $iGlu_f$ and $iGlu_u$ to paired-pulse stimulation (**Fig. 2** and **SI Appendix Fig. S2**) and to trains of 10 action potentials (APs) at 50, 67 and 100 Hz (**SI Appendix Fig. S5**) was tested. While the responses of iGluSnFR and $iGlu_f$ suggested build-up of glutamate during high frequency stimulation, $iGlu_u$ responses revealed that even at 100 Hz stimulation, glutamate was completely cleared from the synaptic cleft between action potentials (**Fig. 2f, SI Appendix Fig. S5i**). Interestingly, the amplitudes of synaptic fluorescence signals ($\Delta F/F_0$) were similar for all three indicators, suggesting that the *on*-rate, not the overall affinity, determined the number of glutamate-bound indicator molecules in the synaptic cleft.

Excitatory postsynaptic potentials (EPSPs) in CA1 become strongly depressed during high-frequency stimulation (17). We were interested whether EPSP depression during 100 Hz stimulation could be fully accounted for by depression of glutamate release from presynaptic boutons. In paired recordings from connected CA3-CA1 pyramidal cells, we triggered APs in the CA3 cell by brief current injections while monitoring postsynaptic potentials (EPSPs) in the CA1 cell. The protocol consisted of a short high frequency burst (10 APs at 100 Hz) followed by a single AP 500 ms after the burst to probe recovery of synaptic function (18). We repeated the protocol up to 100 times at 0.1 Hz and averaged the recorded traces (**Fig. 3a,b,c**). As expected, connected CA3-CA1 pyramidal cell pairs showed strong depression during the high frequency train. The response to the recovery test pulse (#11) was not significantly different from the first EPSP in the train, indicating full recovery of synaptic function. To investigate depression and recovery of glutamate release, we evaluated $iGlu_u$ signals during identical stimulation (**Fig. 3d,e**). Due to the extremely fast kinetics of the indicator, deconvolution of the fluorescence time course was not necessary: we read the peak amplitudes during the 100 Hz train directly from the averaged fluorescence time course (average of 10 individual trials sampled at 1 kHz). Glutamate release decreased during the train with a time course that matched EPSP depression (**Fig. 3d**). This result points to a purely presynaptic origin of depression, which is consistent with AMPA receptors rapidly recovering from desensitization after each release event ($r_{ecovery}$ = 5 ms (19)). However, glutamate release 500 ms after the tetanus was still significantly depressed (two-tailed student's test, *p*-value: 0.0034) while AMPA receptor currents were not. This discrepancy suggests that the response of AMPA receptors to cleft glutamate was in fact potentiated 500 ms after the high frequency train, compensating for the reduced output of Schaffer collateral boutons.

Paired-pulse facilitation correlates with rapid recovery from depression. The rapid kinetics of $iGlu_u$ allowed us to analyze frequency filtering at individual boutons. On the second AP, boutons showed a wide range of facilitated (3 out of 12 boutons) or depressed responses (9 out of 12 boutons, **Fig. 3e**). The response to the tenth AP was strongly depressed in all boutons (16% of response amplitude to first AP), with no correlation between the second and the tenth response (R^2 = 0.005, **Fig. 3f,h**). Interestingly, a highly significant correlation was observed between the response to the second AP and the recovery response 500 ms after the high frequency train (R^2 = 0.715, **Fig. 3g,i**). In contrast, we found no correlation between the amount of bleaching in individ-

ual experiments (F_0(pre-11th pulse)/F_0(pre-1st pulse) and the amplitude of the recovery response ($(^{\triangle}F/F_0)_{11th\ pulse}/(^{\triangle}F/F_0)_{1st\ pulse}$), indicating that poor recovery was not caused by excessive bleaching or dilution of indicator molecules (**Fig. 3j**). Thus, synapses that showed pronounced paired-pulse facilitation were also able to recover rapidly from depression, both of which is indicative of a low utilization of presynaptic resources (18). Such boutons are optimized for the transmission of high-frequency activity (spike bursts). In contrast, boutons that showed paired-pulse depression were still depressed 500 ms after the high-frequency train. These boutons act as low-pass filters: they preferentially transmit isolated APs preceded by a silent period.

Response kinetics of iGluSnFR and variants iGlu$_f$ and iGlu$_u$ are based on the rate of structural change. Finally, we investigated the response mechanism of iGluSnFR and its fast variants using fluorescence stopped-flow with millisecond time resolution. In association kinetic experiments (20 °C), the fluorescence response rates (k_{obs}) showed hyperbolic glutamate concentration dependence, approaching saturating rates of 643 s^{-1} and 1240 s^{-1} for iGluSnFR and iGlu$_f$, respectively (**Fig. 4a-d**). For iGlu$_u$, in contrast, k_{obs} was found to be concentration-independent at 604 s^{-1} (**Fig. 4e,f**). We considered two different reaction pathways to explain our kinetic data (**Fig. 4g**). iGluSnFR is represented as a complex of the large fragment of the GluBP domain (GluBP 1-253, iGlu$_l$), N-terminally flanking cpEGFP and of the C-terminally fused small GluBP fragment (GluBP 254-279, iGlu$_s$). The term iGlu$_l$∼iGlu$_s$, indicates that the large GluBP fragment iGlu$_l$ and the small fragment iGlu$_s$ are within one molecule, albeit separated by the interjecting cpEGFP. In **Scheme 1**, the binding of glutamate to iGlu$_l$ in iGlu$_l$∼iGlu$_s$ is the primary step (no change in fluorescence). Glutamate binding is followed by a conformational change induced by the reattachment of iGlu$_s$ to Glu-bound iGlu$_l$, resulting in the highly fluorescent Glu.iGlu$_c$* complex (rate limiting step). According to **Scheme 1**, the hyperbolic dependence of the observed rate k_{obs} on the glutamate concentration [Glu] has the intercept of the y-axis at k_{-2} (see **SI Appendix Kinetic Theory**, **eq. 7**). At low [Glu], the initial linear slope gives $k_{+2}K_1$. At high [Glu], k_{obs} tends to $k_{+2}+k_{-2}$. Although k_{obs} for iGlu$_u$ appears essentially concentration independent, its kinetics is consistent with **Scheme 1**, with $k_{+2}+k_{-2}$ having a similar value to k_{-2} (**SI Appendix Table S5**).

In the alternative pathway (**Scheme 2**), the reattachment of iGlu$_s$ to iGlu$_l$ occurs without prior binding of glutamate. Therefore, iGlu$_l$∼iGlu$_s$ with the GluBP fragments separated and complete GluBP domain (iGlu$_c$*) are in equilibrium. The conformational change that represents the reattachment of the two GluBP fragments is expected to generate a fluorescent state of cpEGFP. However, the equilibrium is likely to be strongly shifted to the separated, non-fluorescent state (iGlu$_l$∼iGlu$_s$). Assuming that this equilibrium is fast and glutamate binding stabilizes the fluorescent state, at low [Glu], a linear dependence of k_{obs} on [Glu] is predicted with a slope of $K_3k_{+4}/(1+K_3)$ and an intercept of the y-axis at k_{-2} (see **SI Appendix Kinetic Theory**, **eq. 15**). Although at low [Glu], mono-exponential fluorescence changes are expected, as [Glu] increases, the concentration of iGlu$_c$* cannot be assumed to be at steady-state and slow isomerisation will limit k_{obs}, in a similar pattern to that for Scheme 1. Thus, at high [Glu], even if iGlu$_c$* and Glu.iGlu$_c$* have equal relative fluorescence intensities, biphasic fluorescence changes would be expected for the association reactions. As all the reactions studied here for the three variants had a single exponential appearance, we can exclude **Scheme 2** as a possible reaction pathway. In conclusion, **Scheme 1** provides an excellent fit to our measurements (**SI Appendix Table S5**), pointing to 'Venus fly-trap' closure by glutamate binding as a required first step for the conformational change that increases iGluSnFR fluorescence.

Discussion

The development of iGluSnFR was a breakthrough in fluorescent glutamate sensors towards investigating neurotransmission in living organisms (20). Here we describe how to overcome one of the key limitations of iGluSnFR, its slow response kinetics, and use the new utrafast variant iGlu$_u$ to investigate synaptic transmission and frequency filtering at individual Schaffer collateral boutons. For all tested variants, synaptic *off*-kinetics were slower by a factor of 2.5 - 3.8 compared to temperature-matched *in vitro* measurements on isolated protein. This is consistent with the much higher affinities of HEK293T cell-expressed glutamate sensors compared to soluble protein. These systematic differences, also noted in the original characterization of iGluSnFR (12), may be attributed to the tethering of the molecule to a membrane anchor, slowing down conformational changes compared to free-floating sensor molecules. Nevertheless, the relative differences in affinity and kinetics of the new versions compared to iGluSnFR were preserved *in vitro* and *in situ*. The *on*- and *off*-rates of iGlu$_u$ are greater (2- and 5-6 fold, respectively) compared to iGluSnFR. Interestingly, iGlu$_u$ was a faster reporter in the hippocampal slice than iGlu$_f$, even though the latter has a faster limiting *on*-rate. iGlu$_u$ may be put at an advantage over iGlu$_f$ by its concentration-independent response kinetics. It must be noted that the kinetics of iGluSnFR-type indicators are ultimately limited by the structural change that reconstitutes the fluorescent complex, similar to calcium-sensing GCaMPs. The constraints of the mechanism with regard to the onset of fluorescence suggest that it cannot be engineered to resolve sub-millisecond glutamate dynamics. To achieve microsecond response times, it might be necessary to develop hybrid glutamate indicators using synthetic dyes.

Synaptic iGlu$_u$ imaging revealed complete clearance of glutamate between release events even at 100 Hz stimulation frequency. The first attempts to estimate the time course of synaptic glutamate transients were based on the decay of NMDA receptor responses in primary cell culture: kinetic analysis of the displacement of a competitive NMDA receptor antagonist suggested glutamate clearance with τ = 1.2 ms (21). More recent studies using computational modeling and fluorescence anisotropy imaging in tissue suggest that it is closer to 100 µs (22, 23). Thus, due to the intrinsic kinetic limits of the iGluSnFR mechanism, even iGlu$_u$ cannot resolve the true dynamics of free glutamate in the synaptic cleft. Moreover, our spatiotemporal resolution is limited by scanning, even though in most experiments, the spiral scan line intersected the release site two or more times, and thus effectively increased temporal sampling of cleft glutamate by the same factor (e.g. from 1 to 2 kHz). In our analysis, we binned all measurements (pixels) of a scan line into a single time point (1 ms), potentially undersampling the sharp peak of iGlu$_u$ signals (**Fig. S6**). For experiments where the peak amplitude of iGlu$_u$ signals is of critical importance, temporal sampling could be improved by assigning a time value to every pixel of the spiral scan line before ROI analysis (**Fig. S2**). What we can say with confidence is that accumulation of glutamate in the synaptic cleft does not contribute to short-term plasticity at Schaffer collateral synapses.

Glutamate release showed strong depression during 100 Hz firing, in line with the expected depletion of release-ready vesicles. As we controlled the generation of every action potential by somatic current injections, we can exclude decreased afferent excitability as a source of depression in these experiments (17). AMPA receptor currents during 100 Hz firing did not show more run-down than iGlu$_u$ responses, suggesting that AMPA receptor desensitization did not play a major role in the decrease of synaptic efficacy during the train. Paradoxically, AMPA responses were fully recovered 500 ms after the train while the iGlu$_u$ response was still significantly depressed. The most parsimonious explanation is a long-lasting depression of glutamate release. There are al-

ternative scenarios that could explain smaller $iGlu_u$ responses on the 11th pulse, e.g. indicator molecules retrieved into endosomal structures during endocytosis, or accumulation of indicator in a (hypothetical) desensitized state. In these scenarios, facilitating boutons, which experience more exo- and endocytosis and $iGlu_u$ activation during the train, would be expected to show smaller responses at the 11th pulse. However, we found a strong correlation in the opposite direction, making these scenarios less likely.

As response amplitudes (40% - 120% $\Delta F/F_0$) were typically less than half of the maximum change in fluorescence we determined for the three indicators (**SI Appendix Table S3**), we did not correct for the non-linearity of the iGluSnFR variants (**Fig. 1c**). To determine the absolute (or 'peak') glutamate concentration in the synaptic cleft, however, indicator saturation and undersampling would have to be taken into account.

The full recovery of the AMPA response points to an unexpected increase in sensitivity of the postsynaptic compartment to glutamate. By association with different auxiliary proteins and other scaffold-related mechanisms, the density and open probability of postsynaptic glutamate receptors can quickly change (24, 25). In hippocampal slice cultures, post-tetanic potentiation is well established and requires the activity of protein kinase C (26). Thus, it is possible that elevated Ca^{2+} levels in the spine during our high frequency protocol enhanced AMPA receptor currents by a number of mechanisms, compensating for the reduced glutamate release 500 ms after the tetanus.

The surprisingly tight correlation between paired-pulse facilitation and rapid recovery from depression at individual boutons provides direct evidence that differential use of presynaptic resources determines the neural code between pyramidal cells (1, 18). Using Schaffer collateral synapses as an example, we show that $iGlu_u$ is a useful tool for a mechanistic analysis of high frequency synaptic transmission, interrogating presynaptic function independently of postsynaptic transmitter receptors.

METHODS

We provide a detailed description of the methods, data analysis and kinetic modeling in the online Supporting Information. Plasmids for $iGlu_f$, $iGlu_u$ will be deposited at Addgene and made available once the manuscript is accepted for publication.

Materials. pCMV(MinDis).iGluSnFR and pRSET FLIPE-600n plasmids were a gift from Loren Looger (Addgene Plasmid #41732) and Wolf Frommer (Addgene plasmid # 13537), respectively. Site-directed mutagenesis was carried out following the QuikChange II XL protocol (Agilent Technologies).

Fluorescence spectroscopies. Glutamate association and dissociation kinetic experiments of iGluSnFR proteins were carried out on a Hi-Tech Scientific SF-61DX2 stopped-flow system equipped with a temperature manifold (27). Fluorescence spectra and equilibrium glutamate titrations were recorded on a Fluorolog3 (Horiba Scientific).

***In situ* glutamate titration.** HEK293T cells were cultured on 24-well glass bottom plates in DMEM containing non-essential amino-acids (Life Technologies), 10% heat inactivated FBS (Life Technologies) and penicillin/streptomycin (100 U/mL, 100 mg/mL, respectively), at 37 °C in an atmosphere of 5% CO_2. Cells were allowed 24 h to adhere before transfection with Lipofectamine 2000 (Invitrogen). Cells were examined at 37 °C (OKO lab incubation chamber) with a 3i Marianas spinning-disk confocal microscope equipped with a Zeiss AxioObserver Z1, a 40x/NA1.3 oil immersion objective and a 3i Laserstack as excitation light source (488 nm).

Synaptic measurements. Organotypic hippocampal slices (400 µm) were prepared from male Wistar rats at postnatal day 5 as described (28). iGluSnFR and variant plasmids were electroporated into 2-3 CA3 pyramidal cells at 40 ng/µL (iGluSnFR) or 50 ng/µL ($iGlu_f$, $iGlu_u$) together with tdimer2 (20 ng/µL), a cytoplasmic red fluorescent protein (29). 2 - 4 days after electroporation (at DIV 14-30), slice cultures were placed in the recording chamber of a two-photon microscope and superfused with artificial cerebrospinal fluid. Whole-cell recordings from a transfected CA3 pyramidal cell were made with a Multiclamp 700B amplifier (Molecular Devices). Red and green fluorescence was detected through the objective (LUMPLFLN 60XW, 60x, NA 1.0, Olympus) and through the oil immersion condenser (NA 1.4, Olympus) using 2 pairs of photomultiplier tubes (H7422P-40SEL, Hamamatsu).

Acknowledgements. We thank Dr Zoltan Ujfalusi (University of Kent) for assistance with stopped-flow experiments, Iris Ohmert for the preparation of organotypic cultures and Dr David Trentham for comments on the manuscript. Use of The Institute of Translational Medicine, University of Liverpool Imaging Facility is gratefully acknowledged. This project was supported by the Wellcome Trust (Grant 094385/Z/10/Z to K.T.) and BBSRC (Grant BB/M02556X/1 to K.T.); the German Research Foundation (SPP 1665, SFB 936, FOR 2419 to T.G.O; SPP 1926, FOR 2419 to J.S.W) and the European Research Council (ERC-2016-StG 714762 to J.S.W.).

1. Markram H, Wang Y, Tsodyks M (1998) Differential signaling via the same axon of neocortical pyramidal neurons. Proc Natl Acad Sci U S A 95:5323-5328.
2. Regehr WG (2012) Short-term presynaptic plasticity. Cold Spring Harb Perspect Biol 4:a005702.
3. Jenkins MA, Traynelis SF (2012) PKC phosphorylates GluA1-Ser831 to enhance AMPA receptor conductance. Channels (Austin) 6:60-64.
4. Best SL, Török K (2005) Development of a fluorescent glutamate binding protein. Biophysical Journal 88:46a.
5. Chen GQ, Gouaux E (1997) Overexpression of a glutamate receptor (GluR2) ligand binding domain in Escherichia coli: application of a novel protein folding screen. Proc Natl Acad Sci U S A 94:13431-13436.
6. Kuusinen A, Arvola M, Keinanen K (1995) Molecular dissection of the agonist binding site of an AMPA receptor. EMBO J 14:6327-6332.
7. de Lorimier RM, Smith JJ, Dwyer MA, Looger LL, Sali KM, Paavola CD, Rizk SS, Sadigov S, Conrad DW, Loew L, Hellinga HW (2002) Construction of a fluorescent biosensor family. Protein Sci 11:2655-2675.
8. Hu Y, Fan CP, Fu G, Zhu D, Jin Q, Wang DC (2008) Crystal structure of a glutamate/aspartate binding protein complexed with a glutamate molecule: structural basis of ligand specificity at atomic resolution. J Mol Biol 382:99-111.
9. Hires SA, Zhu Y, Tsien RY (2008) Optical measurement of synaptic glutamate spillover and reuptake by linker optimized glutamate-sensitive fluorescent reporters. Proc Natl Acad Sci U S A 105:4411-4416.
10. Okumoto S, Looger LL, Micheva KD, Reimer RJ, Smith SJ, Frommer WB (2005) Detection of glutamate release from neurons by genetically encoded surface-displayed FRET nanosensors. Proc Natl Acad Sci U S A 102:8740-8745.
11. Tsien RY (2005) Building and breeding molecules to spy on cells and tumors. FEBS Lett 579:927-932.
12. Marvin JS, Borghuis BG, Tian L, Cichon J, Harnett MT, Akerboom J, Gordus A, Renninger SL, Chen TW, Bargmann CI, Orger MB, Schreiter ER, Demb JB, Gan WB, Hires SA, Looger LL (2013) An optimized fluorescent probe for visualizing glutamate neurotransmission. Nat Methods 10:162-170.
13. Nakai J, Ohkura M, Imoto K (2001) A high signal-to-noise Ca(2+) probe composed of a single green fluorescent protein. Nat Biotechnol 19:137-141.
14. Baird GS, Zacharias DA, Tsien RY (1999) Circular permutation and receptor insertion within green fluorescent proteins. Proc Natl Acad Sci U S A 96:11241-11246.
15. Taschenberger H, Woehler A, Neher E (2016) Superpriming of synaptic vesicles as a common basis for intersynapse variability and modulation of synaptic strength. Proc Natl Acad Sci U S A 113:E4548-E4557.
16. Zheng K, Rusakov DA (2015) Efficient integration of synaptic events by NMDA receptors in three-dimensional neuropil. Biophys J 108:2457-2464.
17. Kim E, Owen B, Holmes WR, Grover LM (2012) Decreased afferent excitability contributes to synaptic depression during high-frequency stimulation in hippocampal area CA1. J Neurophysiol 108:1965-1976.
18. Tsodyks MV, Markram H (1997) The neural code between neocortical pyramidal neurons depends on neurotransmitter release probability. Proc Natl Acad Sci U S A 94:719-723.
19. Crowley JJ, Carter AG, Regehr WG (2007) Fast vesicle replenishment and rapid recovery from desensitization at a single synaptic release site. J Neurosci 27:5448-5460.
20. Xie Y, Chan AW, McGirr A, Xue S, Xiao D, Zeng H, Murphy TH (2016) Resolution of High-Frequency Mesoscale Intracortical Maps Using the Genetically Encoded Glutamate Sensor iGluSnFR. J Neurosci 36:1261-1272.
21. Clements JD, Lester RA, Tong G, Jahr CE, Westbrook GL (1992) The time course of glutamate in the synaptic cleft. Science 258:1498-1501.
22. Scimemi A, Beato M (2009) Determining the neurotransmitter concentration profile at active synapses. Mol Neurobiol 40:289-306.
23. Zheng K, Jensen TP, Savtchenko LP, Levitt JA, Suhling K, Rusakov DA (2017) Nanoscale diffusion in the synaptic cleft and beyond measured with time-resolved fluorescence anisotropy imaging. Sci Rep 7:42022.
24. Compans B, Choquet D, Hosy E (2016) Review on the role of AMPA receptor nanoorganization and dynamic in the properties of synaptic transmission. Neurophotonics 3:041811.
25. Carbone AL, Plested AJ (2016) Superactivation of AMPA receptors by auxiliary proteins. Nat Commun 7:10178.
26. Brager DH, Cai X, Thompson SM (2003) Activity-dependent activation of presynaptic protein kinase C mediates post-tetanic potentiation. Nat Neurosci 6:551-552.
27. Walklate J, Geeves MA (2015) Temperature manifold for a stopped-flow machine to allow measurements from -10 to +40 degrees C. Anal Biochem 476:11-16.
28. Gee CE, Ohmert I, Wiegert JS, Oertner TG (2017) Preparation of Slice Cultures from Rodent Hippocampus. Cold Spring Harb Protoc 2017(2):pdb.prot094888. doi: 10.1101/pdb.prot094888.
29. Wiegert JS, Gee CE, Oertner TG (2017) Single-Cell Electroporation of Neurons. Cold Spring Harb Protoc 2017(2):pdb.top089714. doi: 10.1101/pdb.top089714.

Supporting Information

Ultrafast glutamate sensors resolve high-frequency release at Schaffer collateral synapses

Nordine Helassa[a1*], Céline D. Dürst[b*], Catherine Coates[a], Silke Kerruth[a], Urwa Arif[a], Christian Schulze[b], J. Simon Wiegert[b], Michael Geeves[c], Thomas G. Oertner[b] and Katalin Török[a2]

[a]Molecular and Clinical Sciences Research Institute, St George's, University of London, London SW17 0RE, UK; [b]Institute for Synaptic Physiology, Center for Molecular Neurobiology Hamburg, Hamburg 20251, Germany; [c]School of Biosciences, University of Kent, Canterbury CT2 7NZ, UK

*These authors contributed equally to this work.

[1]Current address: Department of Cellular and Molecular Physiology, Institute of Translational Medicine, University of Liverpool, Crown Street, Liverpool L69 3BX.

[2]To whom correspondence should be addressed: Dr Katalin Török, Molecular and Clinical Sciences Research Institute, St George's, University of London, London SW17 0RE, UK, Telephone: +442087255832; E-mail: ktorok@sgul.ac.uk

SI Methods

Materials. pRSET FLIPE-600n and pCMV(MinDis).iGluSnFR plasmids were a gift from Loren Looger (Addgene Plasmid #41732) and Wolf Frommer (Addgene plasmid # 13537), respectively. pET41a and pET30b vectors were obtained from Novagen. *E. coli* XL10-Gold and BL21 (DE3) Gold cells were purchased from Invitrogen. Restriction enzymes were obtained from New England Biolabs and T4 DNA ligase from Fermentas.

Cloning of glutamate binding proteins into bacterial expression vectors. The *iGluSnFR* gene was subcloned from pCMV(MinDis).iGluSnFR by restriction-ligation into pET41a (GST-fusion expression vector) at BglII and NotI restriction sites and *ybeJ* encoding GluBP was subcloned from pRSET FLIPE 600n (ECFP-ybeJ-Venus) into pET30b (His-fusion expression vector) at BglII and NotI restriction sites.

Site-directed mutagenesis of iGluSnFR. A series of DNA mutations were performed on pET41a-iGluSnFR. Site-directed mutagenesis was carried out following the QuikChange II XL protocol (Agilent Technologies) using the following primers (5'→3'):
R24K, GGTGTGATTGTCGTCGGTCACAAGGAATCTTCAGTGCCTTTCTCT;
E25A, GTCGTCGGTCACCGTGCATCTTCAGTGCCTTTC;
E25D, GATTGTCGTCGGTCACCGTGATTCTTCAGTGCC;
E25R, GATTGTCGTCGGTCACCGTAGATCTTCAGTGCCTTTCTCT;
S72T, GTAAAACTGATTCCGATTACCACGCAAAACCGTATTCCACTGCTG;
T92A, TTGAATGTGGTTCTACCGCCAACAACGTCGAACGC;
Mutations were confirmed by DNA sequencing (Genewiz).

Expression and purification of genetically encoded glutamate indicator (GEGI) proteins. His-tagged GluBP, GST-fused iGluSnFR and variant proteins were overexpressed in *E. coli* BL21 (DE3) Gold cells. Cells were grown at 37 °C and expression was induced overnight at 20 °C in the presence of 0.5 mM isopropyl thio-β-D-galactoside (IPTG). Cells were resuspended in 50 mM Na^+-HEPES, 200 mM NaCl, pH 7.5 containing one tablet of Complete protease inhibitor cocktail (Roche, Basel, Switzerland) and lysed by sonication on ice (VibraCell, Jencons PLS). For GST-fused proteins, clarified lysates were purified by a single-step GST chromatography (GSTrap, ÄKTA Purifier, GE Healthcare) at 4 °C. The purified protein was eluted in 50 mM Na^+-HEPES, 200 mM NaCl, 10 mM reduced glutathione, pH 7.5. For His-tagged GluBP clarified lysate was purified on a NiNTA column (QIAGEN, ÄKTA Purifier, GE Healthcare) at 4 °C. The purified protein was eluted with a linear gradient of 0-0.5 M imidazole. Purity was assessed by SDS-PAGE (gradient of 6.4% - 20% acrylamide/bisacrylamide) and aliquoted fractions were dialyzed against 50 mM Na^+-HEPES, 200 mM NaCl, pH 7.5 and stored at -80 °C.

Measuring protein concentrations. iGluSnFR and GluBP proteins were highly purified, allowing protein concentration to be determined spectroscopically. The absorption spectra of all iGluSnFR proteins comprised three peaks at wavelengths 280 nm, 400 nm and 497 nm. Protein concentrations were determined with molar extinction coefficients (ε_o) at 280 nm calculated from the amino acid composition using a Nanodrop 1000 spectrophotometer (Thermo Scientific). $\varepsilon_{o(280)}$ of 90690 $M^{-1}cm^{-1}$ for GST-iGluSnFR and 24075 $M^{-1}cm^{-1}$ for His-GluBP was calculated (Gill and von Hippel, 1989).

Equilibrium binding titrations for iGluSnFR proteins. Glutamate affinity assays of iGluSnFR proteins were performed by continuous titration using an automated syringe pump

(ALADDIN 1000, WPI). iGluSnFR and variants at 50-100 nM concentration (50 mM Na^+-HEPES, 100 mM NaCl, 2 mM $MgCl_2$, pH 7.5 at 20°C) were titrated with an appropriate stock solution of glutamate at a 10 μL/min flow rate in a stirred 3 mL cuvette. Fluorescence was measured at 492 nm excitation and 512 nm emission wavelengths using a Fluorolog3 spectrofluorimeter (Horiba Scientific). Fluorescence records were corrected for dilution and photobleaching (0.1%/min). Data were normalized and expressed as bound fraction and glutamate dissociation constant (K_d) and cooperativity (n) were obtained by fitting the data to the Hill equation using GraphPad Prism 7 software. All titrations were performed at least in triplicates and expressed as mean ± SEM. Ligand binding specificity was assessed by titrating iGluSnFR proteins as described above with L-aspartate, L-glutamine, D-serine, GABA and glycine.

Stopped-flow fluorimetry. Glutamate association and dissociation kinetic experiments of iGluSnFR proteins were carried out on a Hi-Tech Scientific SF-61DX2 stopped-flow system equipped with a temperature manifold (Walklate and Geeves, 2015) in the 4 °C to 34 °C temperature range, as specified. Fluorescence excitation was set to 492 nm. Fluorescence emission was collected using a 530 nm cut-off filter. At least 3 shots from 3 replicates were averaged for analysis. Data were fitted to a single exponential to obtain the fluorescence rise or decay rate using KinetAssyst software (TgK scientific).

Association kinetics. The solution containing 1 μM protein in 50 mM Na^+-HEPES, 100 mM NaCl, 2 mM $MgCl_2$, pH 7.5 was rapidly mixed (1:1) with 50 mM Na^+-HEPES, 100 mM NaCl, 2 mM $MgCl_2$, pH 7.5 containing increasing glutamate concentrations (concentrations given are those in the mixing chamber). For the determination of temperature dependence of glutamate association rates, protein samples at 1 μM concentration were mixed as above to give a final glutamate concentration of 1 mM for iGluSnFR, 5 mM for iGluSnFR E25D ($iGlu_f$) and 10 mM for iGluSnFR S72T ($iGlu_u$) in the mixing chamber.

Dissociation kinetics. The solution containing 1 μM protein in 50 mM Na^+-HEPES, 100 mM NaCl, 2 mM $MgCl_2$, pH 7.5 with saturating glutamate (15 x K_d) was rapidly mixed (1:1) with 0.67 mM GluBP in 50 mM Na^+-HEPES, 100 mM NaCl, 2 mM $MgCl_2$, pH 7.5 (concentrations in the mixing chamber). For the determination of temperature dependence of glutamate dissociation rates, protein samples at 1 μM concentration were premixed to give a final glutamate concentration of 0.2 mM for iGluSnFR, 0.5 mM for $iGlu_f$ and 1 mM for $iGlu_u$ in the mixing chamber.

pH sensitivity of iGluSnFR, $iGlu_f$ and $iGlu_u$ proteins. To determine the apparent pK_a for iGluSnFR proteins, a series of buffers were prepared. Depending on their respective pH buffering range, appropriate buffer was used for the measurements (MES for pH 6 - 6.5, HEPES for pH 7 - 8, Tris for pH 8.5 - 9 and CAPS for pH 10). The pH titrations were performed by recording fluorescence spectra in glutamate-free (50 mM Na^+-buffer, 100 mM NaCl, 2 mM $MgCl_2$) or glutamate-saturated (50 mM Na^+-buffer, 100 mM NaCl, 2 mM $MgCl_2$, 1 - 10 mM glutamate) using 1 μM protein in 0.5 pH unit intervals (Fluorolog3, Horiba). Final glutamate concentrations were 1 mM for iGluSnFR, 2 mM for $iGlu_f$ and 10 mM for $iGlu_u$.

Quantum yield determination. The concentration of iGluSnFR proteins was adjusted such that the absorbance at the excitation wavelength (492 nm) was between 0.001 and 0.04. A series of dilutions was prepared in a buffered solution (50 mM Na^+-HEPES, 100 mM NaCl, 2 mM $MgCl_2$, pH 7.5 with either no glutamate or 1 - 10 mM glutamate. Final glutamate concentrations were 1 mM for iGluSnFR, 2 mM for $iGlu_f$ and 10 mM for $iGlu_u$. Fluorescence

spectra were recorded on a Fluorolog3 (Horiba Scientific). GCaMP6f quantum yield measured in Ca^{2+}-saturated buffer was used as a reference ($\Phi_{+Ca^{2+}} = 0.59$) (Chen et al., 2013). Data were plotted as integrated fluorescence intensity as a function of absorbance and fitted to a linear regression with slope S. Quantum yield for iGluSnFR proteins was obtained using the following equation: $\Phi_{protein} = \Phi_{GCaMP6f} \times (S_{protein}/S_{GCaMP6f})$.

***In situ* glutamate titration.** HEK293T cells were cultured on 24-well glass bottom plates in DMEM containing non-essential amino-acids (Life Technologies), 10% heat inactivated FBS (Life Technologies) and penicillin/streptomycin (100 U/ml, 100 mg/ml, respectively), at 37 °C in an atmosphere of 5% CO_2. Cells were allowed 24 h to adhere before transfection with Lipofectamine 2000 (Invitrogen) following the manufacturer's recommendations (1.5 µL Lipofectamine 2000 and 0.5 µg plasmid DNA in 50 µL OptiMEM (Life Technologies)) and maintained for 24 h before being used in experiments. HEK293T cells transfected with iGluSnFR, $iGlu_f$ or $iGlu_u$ were washed with PBS and imaged in 20 mM Na^+-HEPES, 145 mM NaCl, 10 mM glucose, 5 mM KCl, 1 mM $MgCl_2$, 1 mM NaH_2PO_4, pH 7.4. Cells were examined at 37 °C (OKO lab incubation chamber) with a 3i Marianas spinning-disk confocal microscope equipped with a Zeiss AxioObserver Z1, a 40x/NA1.3 oil immersion objective and a 3i Laserstack as excitation light source (488 nm). Emitted light was collected through a 525/30 nm BrightLine® single-band bandpass filter (Yokogawa CSU-X filter wheel) onto a CMOS camera (Hamamatsu, ORCA Flash 4.0; 1152x1656 pixels). Glutamate titrations were carried out using 0 - 10 mM L-glutamate (final concentration). Regions of interest (ROI) were defined by ellipses along each cell membrane. A single ROI was analyzed in each cell. ImageJ was used to process the images. GraphPad Prism 7 was used to plot and fit data with the Hill equation. The number of cells analyzed (n) were between 19 and 41, as specified. Data was expressed as mean ± SEM.

Organotypic slice cultures and single cell electroporation. Organotypic hippocampal slices were prepared from male Wistar rats at post-natal day 5 as described (Gee et al., 2017). Briefly, dissected hippocampi were cut into 400 µm slices with a tissue chopper and placed on a porous membrane (Millicell CM, Millipore). Cultures were maintained at 37 °C, 5% CO_2 in a medium containing 80% MEM (Sigma M7278), 20% heat-inactivated horse serum (Sigma H1138) supplemented with 1 mM L-glutamine, 0.00125% ascorbic acid, 0.01 mg/ml insulin, 1.44 mM $CaCl_2$, 2 mM $MgSO_4$ and 13 mM D-glucose. No antibiotics were added to the culture medium. DNA encoding iGluSnFR and tdimer2 were subcloned into a mammalian expression vector (pCI) under the control of the neuron-specific human synapsin1 promoter. $iGlu_f$ and $iGlu_u$ were generated by site-directed mutagenesis of pCI-synapsin-iGluSnFR using the oligonucleotides for the E25D ($iGlu_f$) and S72T ($iGlu_u$) mutations. Individual CA3 pyramidal cells were transfected by single-cell electroporation (Wiegert et al., 2017a;Wiegert et al., 2017b). iGluSnFR and variant plasmids were electroporated at 40 ng/µl (iGluSnFR) or 50 ng/µl ($iGlu_f$, $iGlu_u$) along with a cytoplasmic red fluorescent protein tdimer2 (20 ng/µl). During electroporation slices were kept in 10 mM Na^+-HEPES, 145 mM NaCl, 25 mM D-glucose, 1 mM $MgCl_2$ and 2 mM $CaCl_2$, pH 7.4.

Electrophysiology. Experiments were performed between DIV 14-30 (2 - 4 days after electroporation). Hippocampal slice cultures were placed in the recording chamber of the microscope and superfused with artificial cerebrospinal fluid (ACSF) containing 25 mM $NaHCO_3$, 1.25 mM NaH_2PO_4, 127 mM NaCl, 25 mM D-glucose, 2.5 mM KCl and (saturated with 95% O_2 - 5% CO_2), 2 mM $CaCl_2$ and 1 mM $MgCl_2$. Whole-cell patch clamp recordings from a transfected CA3 pyramidal neurons were performed with a Multiclamp 700B amplifier (Molecular Devices) under the control of Ephus software written in MATLAB (Suter et al.,

2010). CA3 neurons were held in current clamp and stimulated through the patch pipette by brief electrical pulses (2 - 3 ms and 1500 - 3500 pA current injection) to induce single action potentials. Analog signals were filtered at 6 kHz and digitized at 10 kHz. Patch pipettes with a tip resistance of 3.5 to 4.5 MΩ were pulled with a Narishige PC-10 vertical puller and filled with 10 mM K^+-HEPES, 135 mM K^+-gluconate, 4 mM $MgCl_2$, 4 mM Na^+_2-ATP, 0.4 mM Na^+-GTP, 10 mM Na^+_2-phosphocreatine and 3 mM ascorbate (pH 7.2). Slice experiments were performed at 34°C ± 1°C by controlling the temperature of the ACSF with an in-line heating system and the oil immersion condenser with a Peltier element. Dual patch experiments and $iGlu_u$ measurements (**Fig. 3**) were done under NMDAR block (10 µM CPP-ene) to prevent induction of long-term plasticity during high frequency stimulation.

Two-photon microscopy and data analysis. The custom-built two-photon imaging setup was based on an Olympus BX51WI microscope controlled by a customized version the open-source software package ScanImage (Pologruto et al., 2003) written in MATLAB (MathWorks). We used a pulsed Ti:Sapphire laser (MaiTai DeepSee, Spectra Physics) tuned to 980 nm wavelength to simultaneously excite both the cytoplasmic tdimer2 and the membrane bound iGluSnFR. Red and green fluorescence was detected through the objective (LUMPLFLN 60XW, 60x, NA 1.0, Olympus) and through the oil immersion condenser (NA 1.4, Olympus) using 2 pairs of photomultiplier tubes (PMTs, H7422P-40SEL, Hamamatsu). 560 DXCR dichroic mirrors and 525/50 and 607/70 emission filters (Chroma Technology) were used to separate green and red fluorescence. Excitation light was blocked by short-pass filters (ET700SP-2P, Chroma). ScanImage was modified for the user to freely define the scanning path. Signals from iGluSnFR and fast variants were measured by repeatedly scanning a spiral line across the bouton to maximize the signal-to-noise ratio. iGluSnFR signals were sampled at 500 Hz and $iGlu_f$ and $iGlu_u$ signals were sampled either at 500 Hz or 1 kHz.

Fluorescence was monitored at single Schaffer collateral terminals in CA1 while action potentials were triggered by brief (2 ms) depolarizing current injections into the soma of the transfected CA3 neuron. As the precise orientation of the synaptic cleft on the bouton was unknown to us, we used rapid spiral scans to sample the entire surface of the bouton. A spiral scan covering the entire bouton may hit the diffusing cloud of glutamate just once or several times per line. Typically, the spiral scan line intersected the release site multiple times (**Fig. 1j,k**). To maximize the signal-to-noise ratio in every trial, we assigned a dynamic region of interest (ROI): pixel columns (i.e. spatial positions) were sorted according to the change in fluorescence (ΔF) in each column (**Fig. 1j**, **SI Appendix Fig. S2**). To analyze individual trials, we sorted the columns (corresponding to positions along the scan line) according to their relative increase in fluorescence ($\Delta F/F_0$) and evaluated the top 80% (ROI). In contrast to straight line scans, this method was robust against small movements of the bouton between trials (tissue drift). While 500 Hz sampling was sufficient for iGluSnFR, we increased the scanning speed to 1 kHz to capture the peak of the very brief $iGlu_u$ response (**Fig. 1k**). The peak amplitudes were extracted from the average of 10 trials acquired at 0.1 Hz (**Fig. 3a**). To avoid bleach-related run-down during the train, we normalized each of the 11 peaks by a baseline measurement (F_0) taken just 1 ms before. This strategy was possible since the inter-stimulus interval was 10 ms (500 ms for pulse #11) and τ_{off} was 2.6 ms.

For the peak amplitude measurement of postsynaptic AMPA responses (**Fig. 3a**), we repeated the protocol 70 - 100 times at 0.1 Hz and manually removed trials in which the CA1 neuron received spontaneous synaptic input. In addition, we discarded trials where the patch-clamped CA3 neuron failed to spike in response to a somatic current injection, and averaged the remaining trials. The decay time course of the recovery action potential was fitted with a mono-exponential decay function. This decay time constant was then used to extract the

amplitude of individual responses during the 100 Hz train by deconvolution. Analysis was done in MATLAB and GraphPad Prism.

Data analysis and kinetic modelling. Biophysical experiments were performed at least in triplicates and analysed using GraphPad Prism 7 and KinetAsyst (TgK Scientific) software. Experiments on HEK293T cells were carried out on three independent cultures each. The total number of cells analysed in each condition is given in the figure legends. The software package IBS (http://ibs.biocuckoo.org) was used to display the domain structure glutamate sensors. The PyMOL Molecular Graphics System (2002) by W. L. Delano (https://www.pymol.org/ RRID: SCR_000305) was employed for displaying the crystal structure. Global fitting to kinetic data was performed using DynaFit4 software (http://www.biokin.com/dynafit RRID: SCR_008444) according to the **Schemes 1 & 2**.

Kinetic theory. iGluSnFR is represented as $iGlu_l$~$iGlu_s$, indicating that the N-terminally flanking large GluBP fragment (GluBP 1-253, $iGlu_l$) and the C-terminally fused small GluBP fragment (GluBP 254-279, $iGlu_s$) are within one molecule but separated by the interjecting cpEGFP.

Scheme 1:

$$iGlu_l\sim iGlu_s + Glu \underset{k_{-1}}{\overset{k_{+1}}{\rightleftharpoons}} Glu.iGlu_l\sim iGlu_s \underset{k_{-2}}{\overset{k_{+2}}{\rightleftharpoons}} Glu.iGlu_c^*$$

Glutamate binds to the large domain $iGlu_i$ of GluBP. This is a pre-equilibrium that is described by the following equation:

$$\frac{\partial[Glu.iGlu_l\sim iGlu_s]}{\partial t} = k_{+1}[iGlu_l\sim iGlu_s][Glu] - k_{-1}[Glu.iGlu_l\sim iGlu_s] \quad (1)$$

With the equilibrium constant defined as:

$$K_1 = \frac{k_{+1}}{k_{-1}} \quad (2)$$

The total concentration of iGluSnFR, $[iGluSnFR]_0$ is the sum of all iGluSnFR complexes involved in the scheme.

$$[iGluSnFR]_0 = [iGlu_l\sim iGlu_s] + [Glu.iGlu_l\sim iGlu_s] + [Glu.iGlu_c^*] \quad (3)$$

From this term [$iGlu_i$~$iGlu_s$] is derived as:

$$[iGlu_l\sim iGlu_s] = [iGluSnFR]_0 - [Glu.iGlu_l\sim iGlu_s] - [Glu.iGlu_c^*] \quad (4)$$

If steady-state is assumed for the glutamate-bound iGluSnFR ($Glu.iGlu_l$~$iGlu_s$) then **eq. 1** equals zero and we can insert **eq. 4** to obtain a term for [$Glu.iGlu_l$~$iGlu_s$].

$$[Glu.iGlu_l\sim iGlu_s] = \frac{K_1[Glu]}{1+K_1}\cdot([iGluSnFR]_0 - [Glu.iGlu_c^*]) \quad (5)$$

The formation of the fluorescent state [$Glu.iGlu_c$*] is defined by:

$$\frac{\partial[Glu.iGlu_c^*]}{\partial t} = k_{+2}[Glu.iGlu_l\sim iGlu_s] - k_{-2}[Glu.iGlu_c^*] \quad (6)$$

Inserting **eq. 5** into **eq. 6** and performing a partial differentiation leads to:

$$k_{obs} = \frac{k_{+2}K_1[Glu]}{1+K_1[Glu]} + k_{-2} \quad (7)$$

With the amplitude *A*, the $K_{overall}$ and K_d defined as:

$$A = \frac{k_{+2}K_1[Glu][iGluSnFR]_0}{1+K_1[Glu]}$$

$$K_{overall} = K_1(1 + K_2)$$

$$K_d = \frac{1}{K_o} = \frac{1}{K_1+K_1K_2} \quad (8a,b,c)$$

Scheme 2:

$$iGlu_l{\sim}iGlu_s \underset{k_{-3}}{\overset{k_{+3}}{\rightleftharpoons}} iGlu_c^* + Glu \underset{k_{-4}}{\overset{k_{+4}}{\rightleftharpoons}} Glu.iGlu_c^*$$

$iGlu_l{\sim}iGlu_s$ first forms the complete state $iGlu_c$* that is fluorescent. The pre-equilibrium can be defined as:

$$\frac{\partial[iGlu_c^*]}{\partial t} = k_{+3}[iGlu_l{\sim}iGlu_s] - k_{-3}[iGlu_c^*] \quad (9)$$

With the equilibrium constant defined as:

$$K_3 = \frac{k_{+3}}{k_{-3}} \quad (10)$$

The total concentration of iGluSnFR, $[iGluSnFR]_0$ is the sum of all iGluSnFR complexes involved in the scheme.

$$[iGluSnFR]_0 = [iGlu_l{\sim}iGlu_s] + [iGlu_c^*] + [Glu.iGlu_c^*] \quad (11)$$

From this term $[iGlu_i{\sim}iGlu_s]$ is derived as:

$$[iGlu_l{\sim}iGlu_s] = [iGluSnFR]_0 - [iGlu_c^*] - [Glu.iGlu_c^*] \quad (12)$$

If steady-state is assumed for ($iGlu_c$*) then **eq. 9** equals zero and we can insert **eq. 12** to obtain a term for [$iGlu_c$*].

$$[iGlu_c^*] = \frac{K_3}{1+K_3} \cdot ([iGluSnFR]_0 - [Glu.iGlu_c^*]) \quad (13)$$

The formation of the fluorescent state [$Glu.iGlu_c$*] is defined by:

$$\frac{\partial[Glu.iGlu_c^*]}{\partial t} = k_{+4}[iGlu_c^*][Glu] - k_{-4}[Glu.iGlu_c^*] \quad (14)$$

Inserting **eq. 13** into **eq. 14** and performing a partial differentiation leads to:

$$k_{obs} = \frac{k_{+4}K_3[Glu]}{1+K_3} + k_{-4} \quad (15)$$

With the amplitude *A*, the $K_{overall}$ and K_d defined as:

$$A = \frac{k_{+4}K_3[Glu][iGluSnFR]_0}{1 + K_3}$$

$$K_{overall} = K_3(1 + K_4)$$

$$K_d = \frac{1}{K_o} = \frac{1}{K_3+K_3K_4} \quad (16a,b,c)$$

Reference List

Chen TW, Wardill TJ, Sun Y, Pulver SR, Renninger SL, Baohan A, Schreiter ER, Kerr RA, Orger MB, Jayaraman V, Looger LL, Svoboda K, Kim DS (2013) Ultrasensitive fluorescent proteins for imaging neuronal activity. Nature 499:295-300.

Gee CE, Ohmert I, Wiegert JS, Oertner TG (2017) Preparation of Slice Cultures from Rodent Hippocampus. Cold Spring Harb Protoc 2017:db.

Gill SC, von Hippel PH (1989) Calculation of protein extinction coefficients from amino acid sequence data. Anal Biochem 182:319-326.

Pologruto TA, Sabatini BL, Svoboda K (2003) ScanImage: flexible software for operating laser scanning microscopes. Biomed Eng Online 2:13.

Suter BA, O'Connor T, Iyer V, Petreanu LT, Hooks BM, Kiritani T, Svoboda K, Shepherd GM (2010) Ephus: multipurpose data acquisition software for neuroscience experiments. Front Neural Circuits 4:100.

Walklate J, Geeves MA (2015) Temperature manifold for a stopped-flow machine to allow measurements from -10 to +40 degrees C. Anal Biochem 476:11-16.

Wiegert JS, Gee CE, Oertner TG (2017a) Single-Cell Electroporation of Neurons. Cold Spring Harb Protoc 2017:db.

Wiegert JS, Gee CE, Oertner TG (2017b) Viral Vector-Based Transduction of Slice Cultures. Cold Spring Harb Protoc 2017:db.

Figure S1

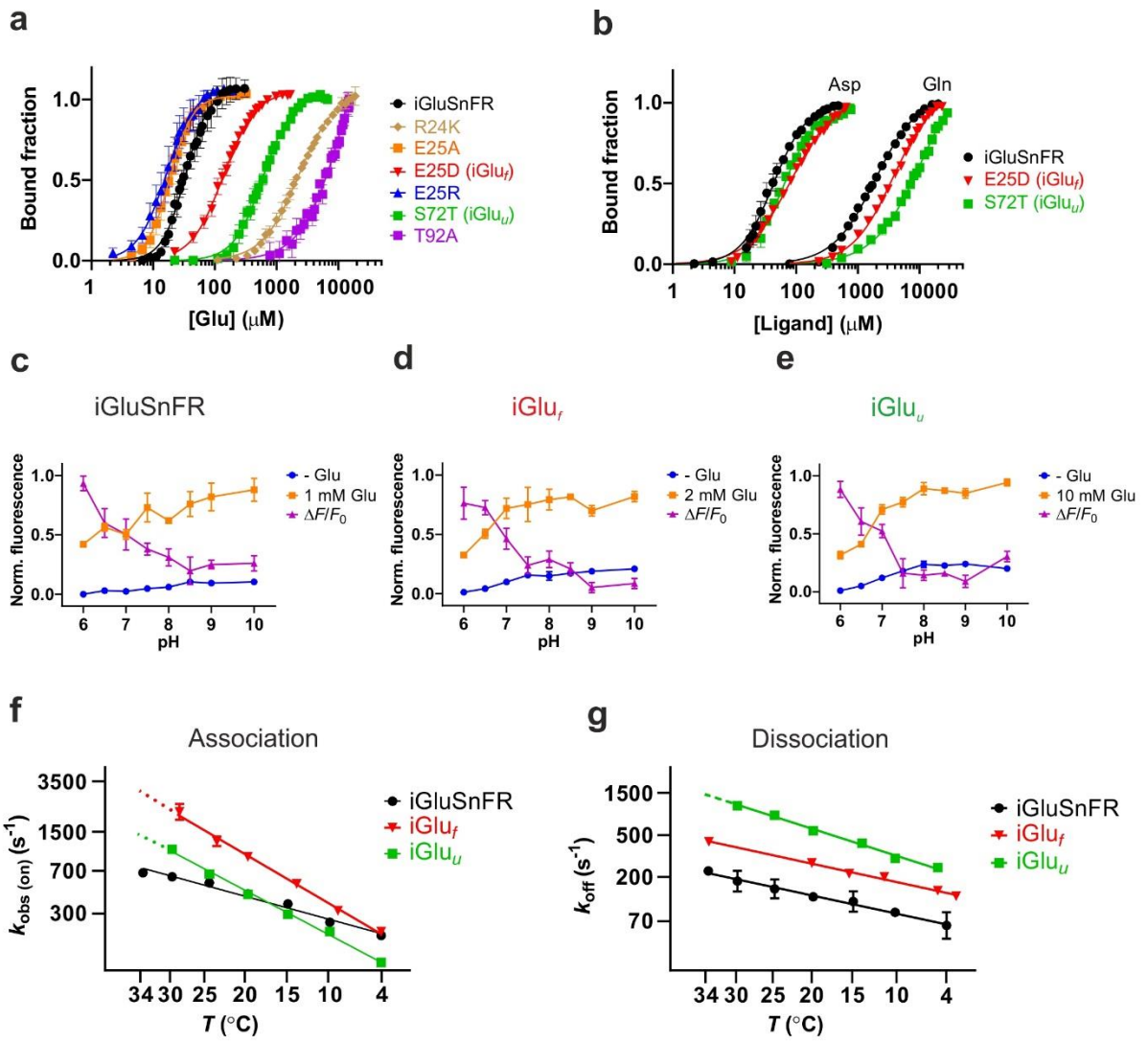

Fig. S1. Biophysical characterization of iGluSnFR variants. (**a**) Equilibrium glutamate binding titrations at 20 °C for iGluSnFR (●), iGluSnFR E25D (iGlu$_f$) (▼), iGluSnFR S72T (iGlu$_u$) (■), iGluSnFR E25R (▲), iGluSnFR E25A (■), iGluSnFR R24K (♦), iGluSnFR T92A (■). Fluorescence changes are normalized to F_0 of 0 and F_{max} of 1. (**b**) Ligand selectivity. Equilibrium titration of iGluSnFR (●), iGlu$_f$ (▼) and iGlu$_u$ (■) with aspartate and glutamine, as indicated. pH sensitivity and pK_a determination of (**c**) iGluSnFR; (**d**) iGlu$_f$; (**e**) iGlu$_u$. Normalized fluorescence in the presence of glutamate (■) (concentration as specified), or in the absence of glutamate (●); $\Delta F/F_0$ (▲). (**f**) Arrhenius plots of the limiting *on*-rates of iGluSnFR, iGlu$_f$ and iGlu$_u$. Values at 34 °C for iGlu$_f$ and iGlu$_u$ are extrapolated assuming the measured slope. (**g**) Arrhenius plot of the dissociation rate constants of iGluSnFR, iGlu$_f$ and iGlu$_u$. The value for iGlu$_u$ 34 °C is extrapolated assuming the measured slope.

Figure S2

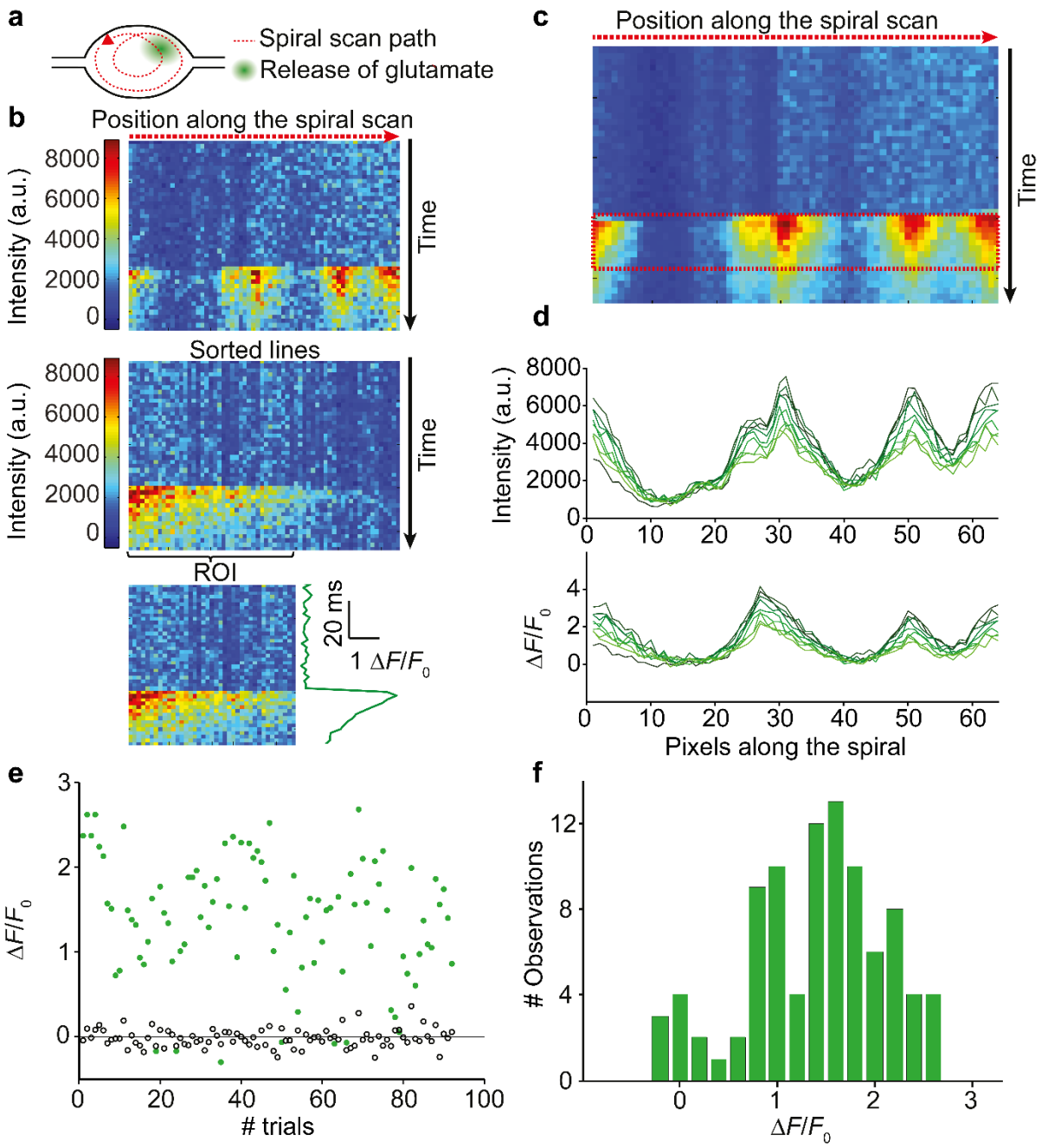

Fig. S2. Extraction of amplitudes from spiral scans. **(a)** Spiral scan intersecting site of vesicular fusion. **(b)** Spiral scan, single trial response. Columns were sorted according to the signal amplitude (ΔF). The region of interest (ROI) was defined as the columns with ΔF > 50% of maximum ΔF (63.2% of maximum for iGlu$_u$). **(c)** Average of 10 trials (single APs) to analyze lateral spread of signal (red box). **(d)** Decay of fluorescence transient (9 scan lines = 18 ms). Note lack of lateral spread of the signal due to slow diffusion of membrane-anchored iGluSnFR. **(e)** iGluSnFR responses from a single Schaffer collateral bouton plotted over time. Single action potential stimulation, (●); No stimulation, (o). Note clear separation of successes and failures. **(f)** Histogram of response amplitudes displayed in panel **(e)**; multiple peaks may be due to multi-vesicular release events.

Figure S3

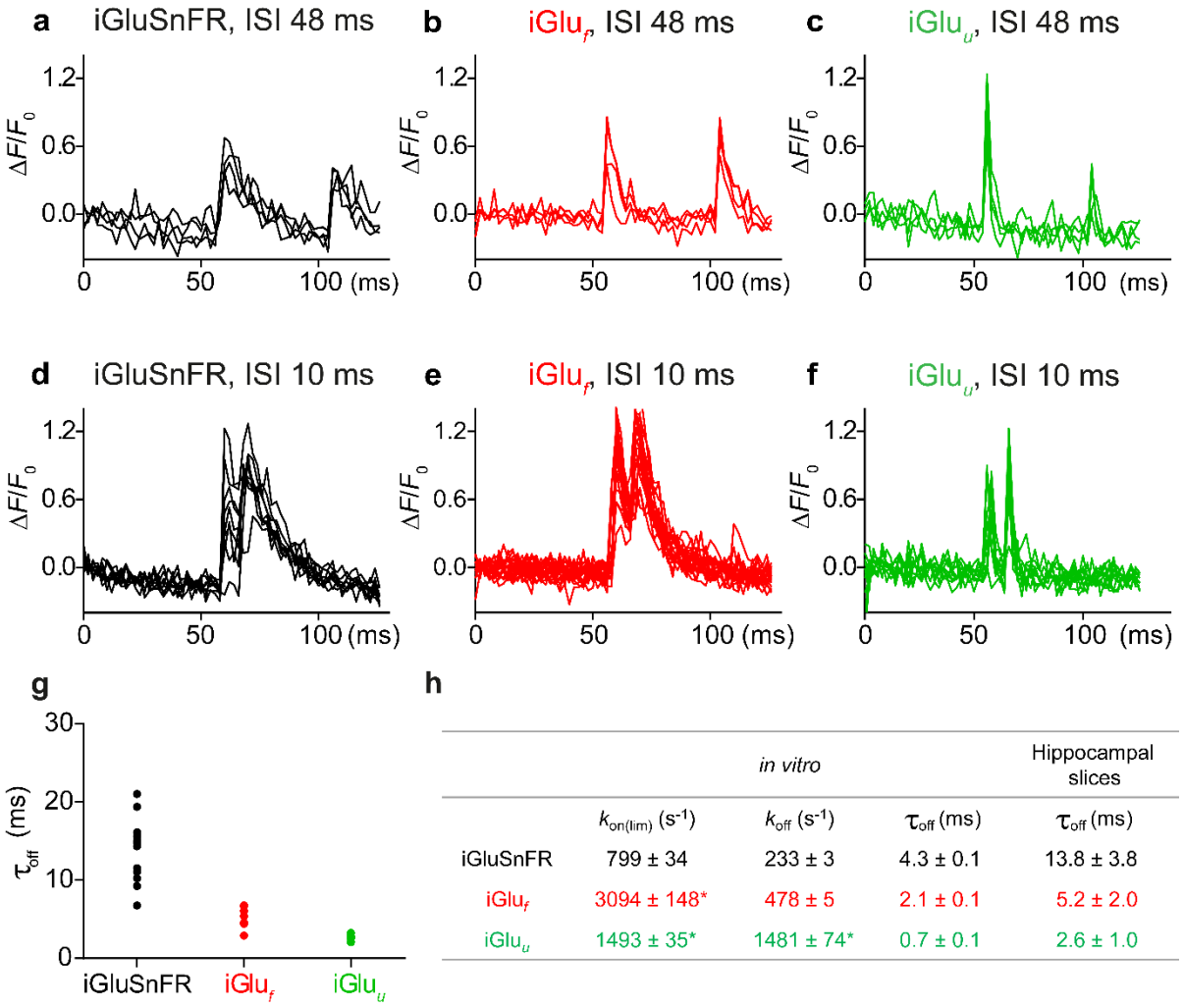

	in vitro			Hippocampal slices
	$k_{on(lim)}$ (s^{-1})	k_{off} (s^{-1})	τ_{off} (ms)	τ_{off} (ms)
iGluSnFR	799 ± 34	233 ± 3	4.3 ± 0.1	13.8 ± 3.8
iGlu$_f$	3094 ± 148*	478 ± 5	2.1 ± 0.1	5.2 ± 2.0
iGlu$_u$	1493 ± 35*	1481 ± 74*	0.7 ± 0.1	2.6 ± 1.0

Fig. S3. Fluorescence time course ($\Delta F/F_0$) in single boutons expressing (**a**) iGluSnFR, (**b**) iGlu$_f$ or (**c**) iGlu$_u$ stimulated by a somatic paired pulse (48 ms ISI). Fluorescence time course ($\Delta F/F_0$) of single boutons expressing (**d**) iGluSnFr, (**e**) iGlu$_f$ or (**f**) iGlu$_u$ stimulated by a somatic paired pulse (10 ms ISI). (**g**) Decay time constant τ_{off} measured in hippocampal slices at 34 ºC for iGluSnFR (n = 13, 500 Hz sampling rate), iGlu$_f$ (n = 7, 1 kHz sampling rate) and iGlu$_u$ (n = 7, 1 kHz sampling rate). (**h**) Summary of *on*- and *off*-rates *in vitro* and decay times measured *in vitro* and in hippocampal slices at 34 ºC. Values are given as mean ± SEM. Values marked by * are extrapolated from Arrhenius plots (**Fig. S1f,g**).

Figure S4

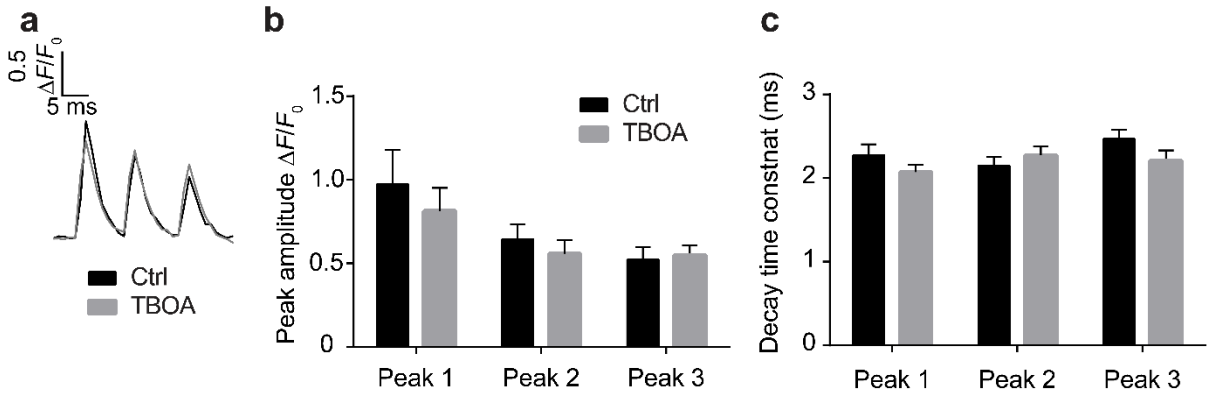

Fig. S4. Testing the effect of glutamate uptake blocker trifluoromethyl-benzoyl-aminophenyl-methoxy-L-aspartic acid (TBOA) on synaptic $iGlu_u$ transients. **(a)** Average traces ($iGlu_u$) from single Schaffer collateral bouton stimulated at 100 Hz, before and after wash-in of TBOA (40 µM). **(b)** Peak amplitude was not affected by TBOA (n = 10 boutons) **(c)** Decay kinetics was not affected by TBOA (n = 10 experiments).

Figure S5

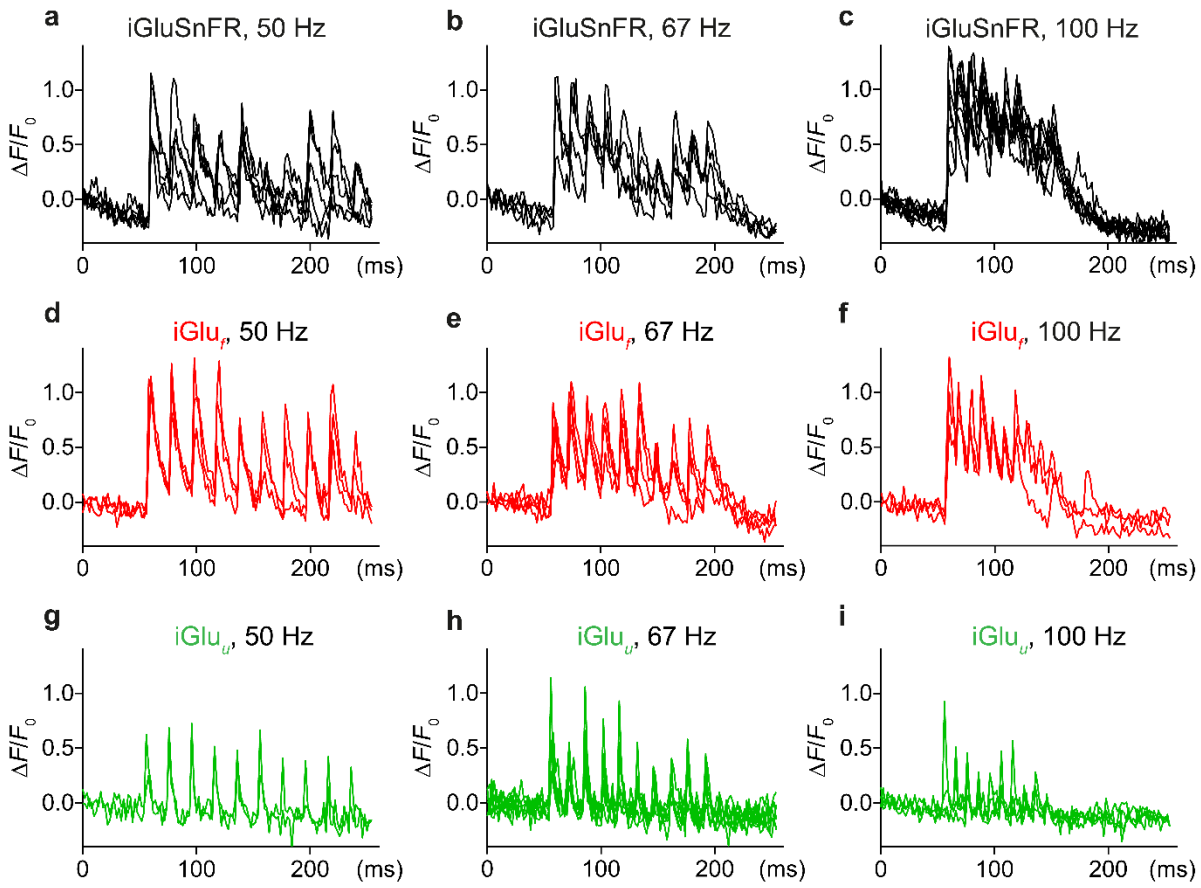

Fig. S5. Fluorescence time course ($\Delta F/F_0$) in single bouton expressing (**a-c**) iGluSnFR, (**d-f**) iGlu$_f$ and (**g-i**) iGlu$_u$ stimulated by 10 APs fired at (**a, d, g**) 50 Hz, (**b, e, h**) 67 Hz and (**c, f, i**) 100 Hz. Number of trials: (**a**), 5; (**b**), 4; (**c**), 8; (**d**), 3; (**e**), 4; (**f**), 3; (**g**), 2; (**h**), 7; (**i**), 4. Depression and recovery of synaptic transmission during 100 Hz trains**.**

Figure S6

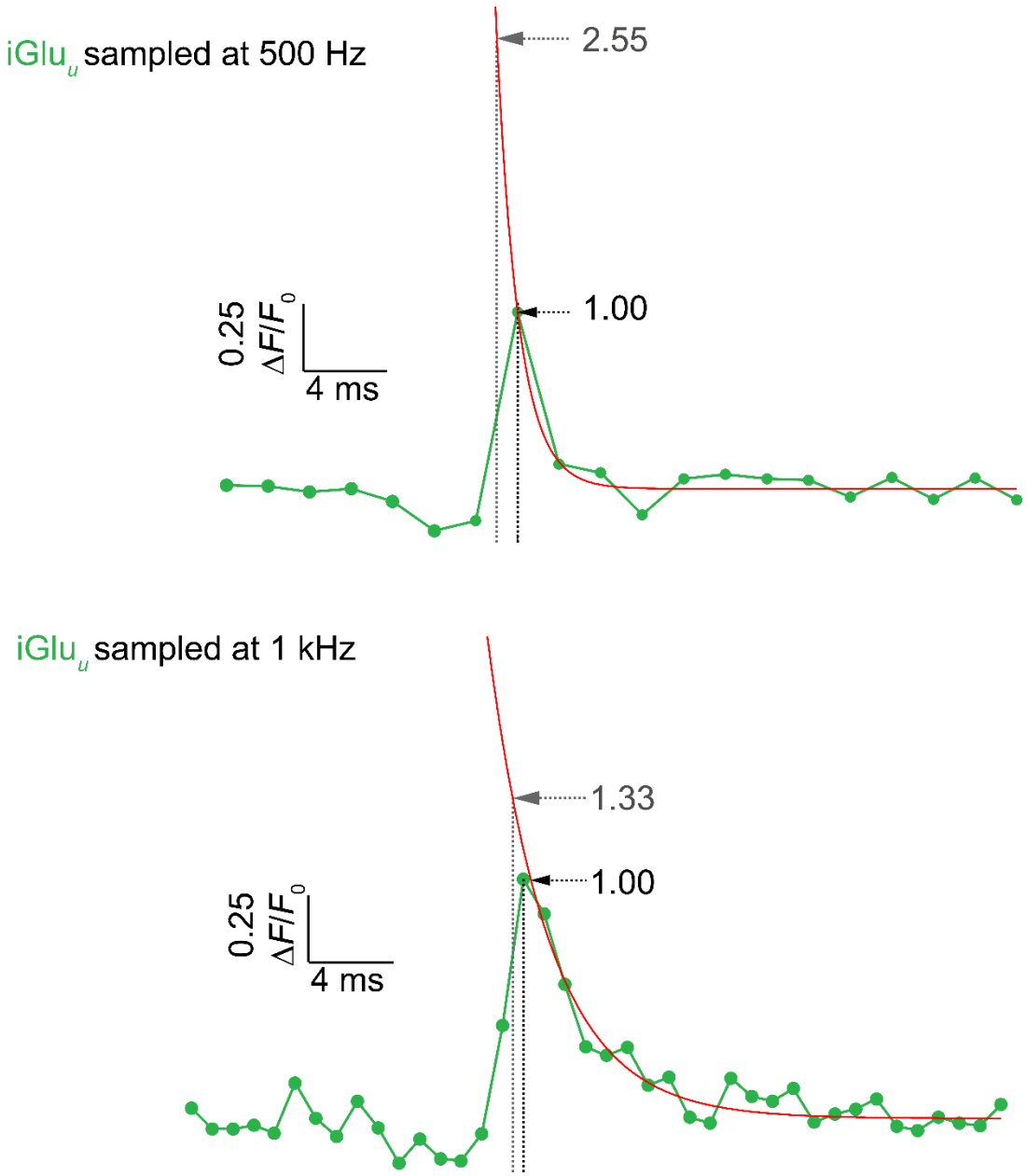

Fig. S6. Estimating peak amplitudes at different sampling frequencies. When sampling iGlu$_u$ fluorescence at 500 Hz, it is possible to miss the peak of the fluorescence transient. Sampling at 1 kHz reduces the potential error to ~33%.

Table S1. Brightness of iGluSnFR variants.

Protein	Φ		$\varepsilon_{o(492nm)}$ ($M^{-1}cm^{-1}$)		Brightness ($mM^{-1}cm^{-1}$)	
	-Glu	+Glu	-Glu	+Glu	-Glu	+Glu
iGluSnFR	0.65 ± 0.02	0.66 ± 0.02	9294 ± 86	38801 ± 293	6.1 ± 0.2	25.4 ± 0.8
$iGlu_f$	0.65 ± 0.02	0.68 ± 0.02	8789 ± 76	28644 ± 127	5.7 ± 0.2	19.4 ± 0.6
$iGlu_u$	0.67 ± 0.02	0.67 ± 0.02	7895 ± 105	22796 ± 120	5.3 ± 0.2	15.3 ± 0.5

Brightness values were obtained from quantum yield and ε_0 measurements.

Table S2. Fluorescence and equilibrium glutamate binding properties of iGluSnFR variants.

Protein	F_r[a] -Glu	F_r[a] +Glu	$F_{r(+Glu)}$ / $F_{r(-Glu)}$	K_d (μM)	*n*
iGluSnFR	1.0	5.4	5.4 ± 0.7	33 ± 0.2	2.3 ± 0.2
S72T (iGlu$_u$)	1.1	4.2	3.8 ± 0.6	600 ± 16	1.8 ± 0.1
E25D (iGlu$_f$)	1.8	7.2	4.0 ± 0.3	137 ± 4	1.7 ± 0.1
E25A	3.6	12.3	3.4 ± 0.6	18.6 ± 0.02	2.6 ± 0.1
E25R	4.7	7.3	1.6 ± 0.5	19.3 ± 0.8	2.3 ± 0.2
R24K	1.5	3.1	2.1 ± 0.1	(2.3 ± 0.1) x 10^3	1.5 ± 0.1
T92A	0.7	1.2	1.7 ± 0.5	(12 ± 4) x 10^3	1.3 ± 0.2

[a]Relative fluorescence values were determined using apo-iGluSnFR as reference (F_r = 1).

Table S3. Selectivity of iGluSnFR, $iGlu_f$ and $iGlu_u$ for L-aspartate and L-glutamine.

Protein	$F_{(+Asp)}/F_{(-Asp)}$	$K_{d(Asp)}$ (μM)	*n*	$F_{(+Gln)}/F_{(-Gln)}$	$K_{d(Gln)}$ (μM)	*n*
iGluSnFR	4.7 ± 0.3	44.6 ± 0.3	1.6 ± 0.1	6.4 ± 0.8	1900 ± 100	1.3 ± 0.1
$iGlu_f$	2.7 ± 0.2	82.0 ± 0.6	1.2 ± 0.1	5.6 ± 0.5	3700 ± 100	1.3 ± 0.1
$iGlu_u$	1.6 ± 0.2	61.7 ± 0.4	1.7 ± 0.1	2.3 ± 0.3	10800 ± 300	1.1 ± 0.1

[a]Fluorescence dynamic range is reported as fold enhancement by aspartate or glutamine ligand binding.

Table S4. Kinetic properties of fast iGluSnFR variants iGlu$_f$ and iGlu$_u$.

Protein	K_d (μM)	n	$k_{on(lim)}$ (s^{-1})	$t_{1/2(on)(lim)}$ (ms)	k_{off} (s^{-1})	$t_{1/2(off)}$ (ms)
iGluSnFR	33 ± 0.2	2.3 ± 0.2	643 ± 23	1.1 ± 0.04	110 ± 4	8.5 ± 0.4
E25D (iGlu$_f$)	137 ± 4	1.7 ± 0.1	1240 ± 77	0.6 ± 0.04	283 ± 36	2.4 ± 0.3
S72T (iGlu$_u$)	600 ± 16	1.8 ± 0.1	604 ± 12	1.1 ± 0.02	468 ± 58	1.5 ± 0.2

K_d and Hill coefficient (n) values were obtained from the equilibrium glutamate titrations at 20 °C. Fluorescence rise (limiting rate, $k_{on(lim)}$) and decay (k_{off}) rates were measured by glutamate association and dissociation stopped-flow kinetic experiments.

Table S5. Fitted and modelled kinetic parameters of the fluorescence response of iGluSnFR variants.

Scheme 1	K_1 (M^{-1})	K_2	$K_{d(calculated)}$ (M)	k_{+1} ($M^{-1}s^{-1}$)	k_{-1} (s^{-1})	k_{+2} (s^{-1})	k_{-2} (s^{-1})	K_1k_{+2} ($M^{-1}s^{-1}$)	$K_{d(measured)}$ (M)	n
iGluSnFR (20 °C)	3642	5.2	3.6×10^{-5}	2.7×10^{7}	5965	569	110	2.1×10^{6}	3.3×10^{-5}	2.3
iGluSnFR (34 °C)	3431	3.4	6.6×10^{-5}	2.8×10^{7}	8161	756	220	2.6×10^{6}	4.0×10^{-5}	1.7
Glu_f (20 °C)	1568	2.35	1.47×10^{-4}	3.5×10^{6}	2206	944	283	1.5×10^{6}	1.37×10^{-4}	1.7
$iGlu_u$ (20 °C)	1291	0.29	6.00×10^{-4}	2.2×10^{6}	1704	136	468	1.7×10^{5}	6.00×10^{-4}	1.8

Fitted parameters to the kinetic model illustrated in **Fig. 4g** are shown for iGluSnFR and fast variants. Fitting the association kinetic records to **Scheme 1** (**SI Methods**, **Kinetic Theory**) gives parameters for a hyperbole, K_1, $k_{+2} + k_{-2}$, k_{-2} and the initial gradient, the apparent association rate constant K_1k_{+2}. Values for k_{+1} and k_{-1} were obtained by global fitting using Dynafit and represent a lower limit of values. The measured and calculated overall K_d values were in good agreement.